ELSEVIER

A comprehensive indoor–outdoor urban climate model with hydrology: The Vertical City Weather Generator (VCWG v2.0.0)

Mohsen Moradi [a], E. Scott Krayenhoff [b], Amir A. Aliabadi [a,*]

[a] School of Engineering, University of Guelph, Guelph, Ontario, Canada
[b] School of Environmental Sciences, University of Guelph, Guelph, Ontario, Canada

ARTICLE INFO

ABSTRACT

Urban climate models can predict the environmental impacts of urban development by simulating the exchange processes between the atmosphere and urban surfaces. A comprehensive simulation of urban climate requires adequate representation of the exchanges of momentum, heat, and water between the atmosphere and the impervious, vegetated, or soil surfaces. This study presents the inclusion of hydrological processes in a computationally-efficient urban micro-climate model, the Vertical City Weather Generator (VCWG v2.0.0). VCWG v2.0.0 accounts for not only the interaction between indoor and outdoor environments through parameterizations including building energy, surface energy balance, radiation, and vertical diffusion models, but also the biophysical and ecophysiological behavior of urban vegetation via an advanced hydrology model. VCWG v2.0.0 is evaluated against field measurements from Basel, Switzerland, in 2002, and Vancouver, Canada, in 2008. The model outperforms the previous version by reducing the RMSE of potential temperature, wind speed, and specific humidity by 0.5 K, 0.52 m s^{-1}, and 0.001 kg kg^{-1}, respectively. Inclusion of the hydrology model also improves prediction of sensible/latent heat fluxes with RMSE of 18.1/27.7 W m^{-2} for the Vancouver case. VCWG v2.0.0 is further assessed by explorations related to seasonal variations, modification of ground vegetation, green and cool roofs, and changes in the Local Climate Zone (LCZ), which are all in reasonable agreement with models and observations in previous studies. VCWG v2.0.0 can be used as a design, prediction, or investigation tool to understand how urban climate variables are influenced as a function of forcing environmental conditions and urban configurations.

1. Introduction

Urban expansion and conversion of the Earth's surface for urban uses have brought numerous environmental issues at various scales. Cities and industrial areas disturb the natural water cycle and thermal energy exchange between the earth surface and the atmosphere. In addition, these areas release anthropogenic pollutants into the atmosphere with negative impacts from local to global scales.

The Urban Heat Island (UHI) is recognized as one of the clearest examples of climate modification caused by replacing natural areas with artificial surfaces. This phenomenon causes greater temperatures in cities compared to their surrounding rural areas. Built-up areas make changes to the energy balance at the lower atmospheric layer (roughness sublayer), which are identified as the main causes of UHI [1]. The UHI is mainly attributed to the reduction in loss of longwave radiation at street level, increased heat storage, anthropogenic heat released from human activities, urban greenhouse effect, radiation trapping

within the urban areas, and loss of evaporation from surfaces compared to vegetated surfaces [2], all of which affect energy performance of buildings [3]. Urbanization generally includes vegetation removal and increases in soil aridity, which reduce the available area for infiltration and increase surface runoff. These modifications can threaten to reduce the amount of groundwater, and ultimately increase demand to import water from distant sources by developing significant network of channels and pipes. So, built-up environments require careful design of drainage systems to cope with the increase in volume and speed of surface runoff [4].

To capture the physical processes occurring in the urban environment, various urban atmospheric models have been developed. Modeling the interaction between urban elements (e.g. trees, buildings, vehicles) and their impacts on energy and water exchanges can help urban planners develop cities more sustainably for climate control, reduced flooding, and improved air quality. Urban climate models are

---

* Corresponding author.
  E-mail address: aliabadi@uoguelph.ca (A.A. Aliabadi).
  URL: https://www.aaa-scientists.com (A.A. Aliabadi).

generally designed for certain spatial and temporal scales that cover the atmospheric processes of interest. For example, if the model aims to determine the exchange processes within an entire city and the atmosphere, the computational domain should be extended far beyond the horizontal and vertical size of the city. Depending on the scale of analysis, the surface representation can vary from a simple one-dimensional slab in a meso-scale model to more realistic forms that include vertical and horizontal dimensions. In meso-scale models, surface–atmosphere interactions are parameterized using urban aerodynamic roughness lengths [5] or adding source/sink terms in the momentum (drag) and energy (anthropogenic heat) equations [6]. While Computational Fluid Dynamics (CFD) models are used for flow analysis in the urban environment, they do not include many meteorological processes (e.g. clouds and precipitation), and they are not computationally efficient [7–13].

Development of Urban Canopy Models (UCMs) has been undertaken with different levels of complexity. These models incorporate physically- or empirically-based parameterizations for radiative, momentum, heat, and moisture exchanges within and above the built-up areas [9,14–21], which make them computationally efficient. The urban canopy can be simplified into a slab or more realistically into two and three-dimensional structures, which describe the thermal and aerodynamic characteristics of the urban canyon. The single-layer models solve the equilibrium equations for each urban facet as they interact with air state variables at a single hypothetical point. The single-layer models, such as the Urban Weather Generator (UWG) [22] and Canyon Air Temperature (CAT) [23], are designed to calculate the climate variables in one layer, which is representative of a neighborhood [15,22,24–27]. These models are usually forced by standard data from a nearby meteorological station. Other models such as the Town Energy Balance (TEB) [28] and Temperatures of Urban Facets-3D (TUF-3D) [29] are forced by meteorological data at the top of the urban domain to solve energy balance equations for urban facades. Multi-layer models, such as Building Effect Parametrization-Tree (BEP-Tree) [30], provide higher resolution in the vertical direction. Multi-layer models solve the energy, mass, and momentum equations at multiple layers extending from ground up to an elevation above canopy height. There is a reciprocal relationship between the buildings and the outdoor environment in forms of drag, which can alter the flow pattern [31–33], and heat exchanges through infiltration, exfiltration, ventilation, walls, roofs, roads, windows, and building energy systems [25,34,35]. In an effort to couple the indoor and outdoor environments, the indoor–outdoor Building Energy Simulator (TUF-3D-IOBES) [35], the Building Effect Parametrization-Building Energy Model (BEP-BEM) [25], and the UWG model have been developed with different levels of complexity.

Some efforts have begun to develop multi-scale climate models by coupling meso-scale and the micro-scale models [36–39]. Meso-scale models are generally coupled with either single-layer or multi-layer canopy models for simulation of urban climate. The coupling approach between the Weather Research and Forecasting (WRF) model and its urban canopy models has been extensively used for weather predictions, regional climates, air quality, and water resources investigations. Different parameterizations have attempted to provide this coupling such as the Noah land-surface model, the Single-Layer Urban Canopy Model (SLUCM) [14,15], and the multi-layer urban canopy model [17,25,40].

Trees and low vegetation (at roof and street levels) can help cool the environment [41,42] and improve the building energy performance [43–45]. Urban plants create these favorable environmental conditions through increasing the latent heat flux and subsequently reducing the sensible heat flux, altering overall albedo of a city, and providing more shaded areas. Parameterization of these effects has been made from a bulk representation of vegetation in UWG to multi-layer representation of trees in BEP-Tree.

Precipitation is known as the primary driver of land surface hydrological processes and a major component in water and energy circulations [46]. In recent years, this recognition has motivated efforts to include urban hydrology in UCMs. The Environment and Climate Change Canada (ECCC) has developed the Soil, Vegetation, and Snow (SVS) scheme. SVS uses the tiling approach, and instead of a single energy budget for the entire surface, separate energy budgets for bare ground, vegetation, and snow cover are considered [47]. Wang et al. [48] developed an urban hydrological model, which was coupled to an urban canopy model, accounting for water transport from natural and engineered surfaces. Recently, the SLUCM in WRF was modified by integration of anthropogenic latent heat, urban irrigation, evaporation from paved surfaces, and the urban oasis effect [49]. Yang et al. [49] evaluated the new WRF-SLUCM model and found that the model prediction underestimates precipitation in the summer and overestimates it in the fall. The results from this coupled model indicated that hydrological processes decrease air temperature and increase dew point temperature in the urban areas and there is a complex relationship between surface temperature and 2-m air temperature. Järvi et al. [46] developed the Surface Urban Energy and Water Balance Scheme (SUEWS), which calculates energy and water balances in the urban area with multiple surface types using hourly meteorological forcing data. The Urban Tethys-Chloris (UT&C) model [50] has shown that the biophysical and ecophysiological behavior of urban vegetation can be a major contributor to urban energy and water balances.

An overview of the literature reveals a lack of an independent urban micro-climate model that accounts for unique features of the built-up environment including building energy, urban energy exchange, urban hydrology, low and high vegetation, and most importantly the dynamic interactions between these elements. To address this need, the Vertical City Weather Generator (VCWG v1.3.2) was developed [51]. VCWG v1.3.2 is a computationally-efficient urban micro-scale and multi-physics simulation platform that predicts temporal and vertical variation of potential temperature, wind speed, specific humidity, and turbulence kinetic energy in the outdoor environment, temperatures on the indoor and outdoor surfaces, temporal variation of building performance metrics such as indoor air temperature and specific humidity, sensible cooling/heating loads, humidification/dehumidification loads, and additional variables [51]. While evaluation and various explorations conducted on VCWG v1.3.2 suggested reasonable performance of the model compared to the previous studies, the model still lacks an appropriate representation of hydrological processes that occur in built-up areas. Thus, inclusion of hydrological processes in VCWG is the primary focus of this study.

1.1. Objectives

The present contribution develops the next version of VCWG v2.0.0, which consists of not only the previous essential components, but also an urban hydrology model. The new version simulates the hydrological processes including evapotranspiration from low and high vegetation at the roof and ground levels, soil evaporation, runon, surface runoff, and infiltration. In addition to the capability to be forced near ground at a nearby rural site, VCWG v2.0.0 can also be forced at the top of the urban domain, which offers the opportunity to investigate the simulation output variables on a spatial grid of the urban environment. The advantages of VCWG over other urban canopy models are (1) the addition of the building energy model and all the detailed physics related to the calculation of building performance metrics such as waste heat of buildings and building load calculation, (2) the ability to resolve vertical profiles of climate variables, which makes the model suitable for assessment of high-rise urban areas, and (3) the versatility of the rural climate forcing based on either Monin–Obukhov Similarity Theory (MOST) or top forcing. The model components and alternative features of VCWG make it a comprehensive, computationally-efficient, and accurate urban canopy model.

In this article, Section 2 provides detailed description of the model components. In Section 3.1, VCWG v2.0.0 is evaluated for its ability to predict meteorological state variables and sensible/latent heat fluxes

against the observations of the Basel UrBan Boundary Layer Experiment (BUBBLE) conducted in Basel, Switzerland, in 2002, and the Sunset neighborhood field measurements conducted in Vancouver, Canada, in 2008. Section 3.2 presents explorations of the model's sensitivity and performance in response to seasonal variations, modified levels of vegetation, roof technologies, and changes in the local climate zone. Finally, the summary of the findings and suggestions for future model developments are discussed in Section 4.

2. Methodology

Fig. 1 shows the VCWG v2.0.0 model schematic. VCWG v2.0.0 consists of six integrated sub-models, coupled to predict vertical profiles of climate variables within the urban area from ground up to multiple times of average buildings height, building energy performance metrics, and surface variables:

1. A rural model forces meteorological boundary conditions on the urban components of the model based on a rural surface energy balance model and the vertical profiles of climate variables in the rural area;
2. An urban one-dimensional vertical diffusion model calculates the vertical profiles of meteorological variables in the urban area considering the effects of momentum, heat, and water exchanges due to the urban elements. This model is forced at the top of the domain either by the rural model, which in turn is forced near the surface and calculates the forcing variables on top of the urban domain, or directly by a top meteorological forcing dataset. This model is also bounded at the bottom by surface energy and water balances;
3. A building energy model calculates the building energy fluxes, energy loads, and waste heat of buildings ejected into the urban environment;
4. A radiation model with trees computes the longwave and shortwave radiation fluxes exchanged with the urban canyon surfaces, trees, and the sky;
5. An urban surface energy balance model calculates surface heat fluxes including sensible, latent, and conductive heat fluxes. The moisture sinks/sources include not only evapotranspiration from tree foliage but also the wet surfaces and soil columns, which contribute to the urban energy balance;
6. An urban hydrology model obtains ecophysiological behavior of urban trees and low vegetation at the ground and roof levels and calculates the urban hydrological exchanges and the soil water content profile in the presence of precipitation.

The rural model requires a deep soil temperature, other meteorological variables near the ground, such as temperature, humidity, wind speed, precipitation, and incident shortwave and longwave radiation fluxes. These variables can be supplied from an EnergyPlus Weather (EPW) file. As an alternative to the rural model, VCWG can read an external forcing file containing wind speed, wind direction, temperature, humidity, and precipitation on an hourly basis at the top of the urban domain. This option is particularly useful when the user wants to couple VCWG with a meso-scale model. For example, if EPW datasets are not available for the region of interest, alternatively VCWG can retrieve forcing data from the ERA5-Land dataset. ERA5-Land is a real-time reanalysis dataset that provides hourly atmospheric variables with a spatial resolution of 9 km from 1981 to present. The model assumes that the internal urban boundary layer has developed sufficiently to be in equilibrium with the underlying urban surface, and the top of the domain is above the urban boundary layer. While forced by the rural model or an external forcing file, the urban one-dimensional vertical diffusion model is also coupled with the building energy, radiation, surface energy balance, and hydrology models. The five models are fully interactive with each other. The coupling between

these models is designed to update the boundary conditions, surface temperatures, and the source/sink terms in the transport equations in successive time step iterations. More details about the models are provided in the subsequent sections and by Moradi et al. [51]. Since this study provides an update of the earlier version of VCWG v1.3.2, the focus of the methodology is on the new parameterizations, while pre-existing formulations are not discussed in detail and can be found in the Appendix or elsewhere [51].

2.1. Rural model

The rural model reads the forcing meteorological variables including wind speed, temperature, and relative humidity near the ground, incoming shortwave and longwave radiation from sky and possibly precipitation. It then calculates the vertical profiles of potential temperature and specific humidity using Monin–Obukhov Similarity Theory (MOST) [51–54]. The rural surface energy balance model is based on the Penman–Monteith (PM) method [55,56]. Deep soil temperature and surface sensible and latent heat fluxes are used to solve the transient heat diffusion equation and ultimately determine the surface temperature. The surface energy balance for the rural area involves the balance of net allwave radiation fluxes $S_{n,rur} + L_{n,rur}$ [W m^{-2}] with sensible H_{rur} [W m^{-2}], latent LE_{rur} [W m^{-2}], and ground conductive G_{rur} [W m^{-2}] heat fluxes,

$$S_{n,rur} + L_{n,rur} = H_{rur} + LE_{rur} + G_{rur}, \tag{1}$$

where the net shortwave radiation flux $S_{n,rur}$ [W m^{-2}] can be calculated as a function of incoming shortwave radiation flux and vegetation coverage, the net longwave radiation flux $L_{n,rur}$ [W m^{-2}] can be calculated as a function of incoming longwave radiation flux and surface temperature, and the sensible heat flux can be calculated using the formulation of Louis [57] and Moradi et al. [51].

Evapotranspiration in an open area covered by low vegetation depends on meteorological quantities (including solar radiation, air temperature, vapor pressure deficit, wind speed near the ground), and types of vegetation, which have different transpiration rates. For an area with low leaf area index, the water is mainly lost by the soil evaporation as the soil surface is exposed to the atmosphere at a larger area. However, rural areas with high vegetation index provide more coverage of the ground underneath, so the transpiration becomes dominant. Based on the PM method, the latent heat flux can be calculated as [58]

$$LE_{rur} = \frac{\Delta(S_{n,rur} + L_{n,rur} - G_{rur}) + \frac{\rho.C_p.VPD}{r_a}}{\Delta + \gamma_1(\frac{r_a + r_s}{r_a})}, \tag{2}$$

where G_{rur} [W m^{-2}] can be calculated as a fraction of the net allwave radiation flux, $\gamma_1 = 0.00163 P_b/L$ [kPa K^{-1}] is the psychrometric constant and can be calculated as a function of barometric pressure P_b [kPa] and latent heat of vaporization L [J kg^{-1}], C_p [J kg^{-1} K^{-1}] is air specific heat capacity, VPD [kPa] is vapor pressure deficit, r_a [s m^{-1}] is aerodynamic resistance, r_s [s m^{-1}] is surface resistance, and Δ [kPa K^{-1}] is the slope of saturated vapor pressure.

Potential temperature $\overline{\Theta}_{rur}$ [K] and specific humidity $\overline{Q}_{rur}$ [kg kg^{-1}] at the top of the domain are required to force the urban model. Vertical profiles of these climate variables in the rural area are calculated using MOST. In MOST, the gradients of potential temperature/specific humidity are functions of sensible/latent heat fluxes at the surface, temperature/humidity roughness lengths $z_{\overline{\Theta},rur}/z_{\overline{Q},rur}$ [m], and friction velocity u_* [m s^{-1}]. The rural model also computes a rural friction velocity using MOST, given the aerodynamic roughness length $z_{0,rur}$ [m], wind speed $\overline{S}_{rur}$ [m s^{-1}], and the universal wind shear function. This friction velocity is used to calculate a source term for the one-dimensional momentum equation. The details of parameterizations are provided by Moradi et al. [51].
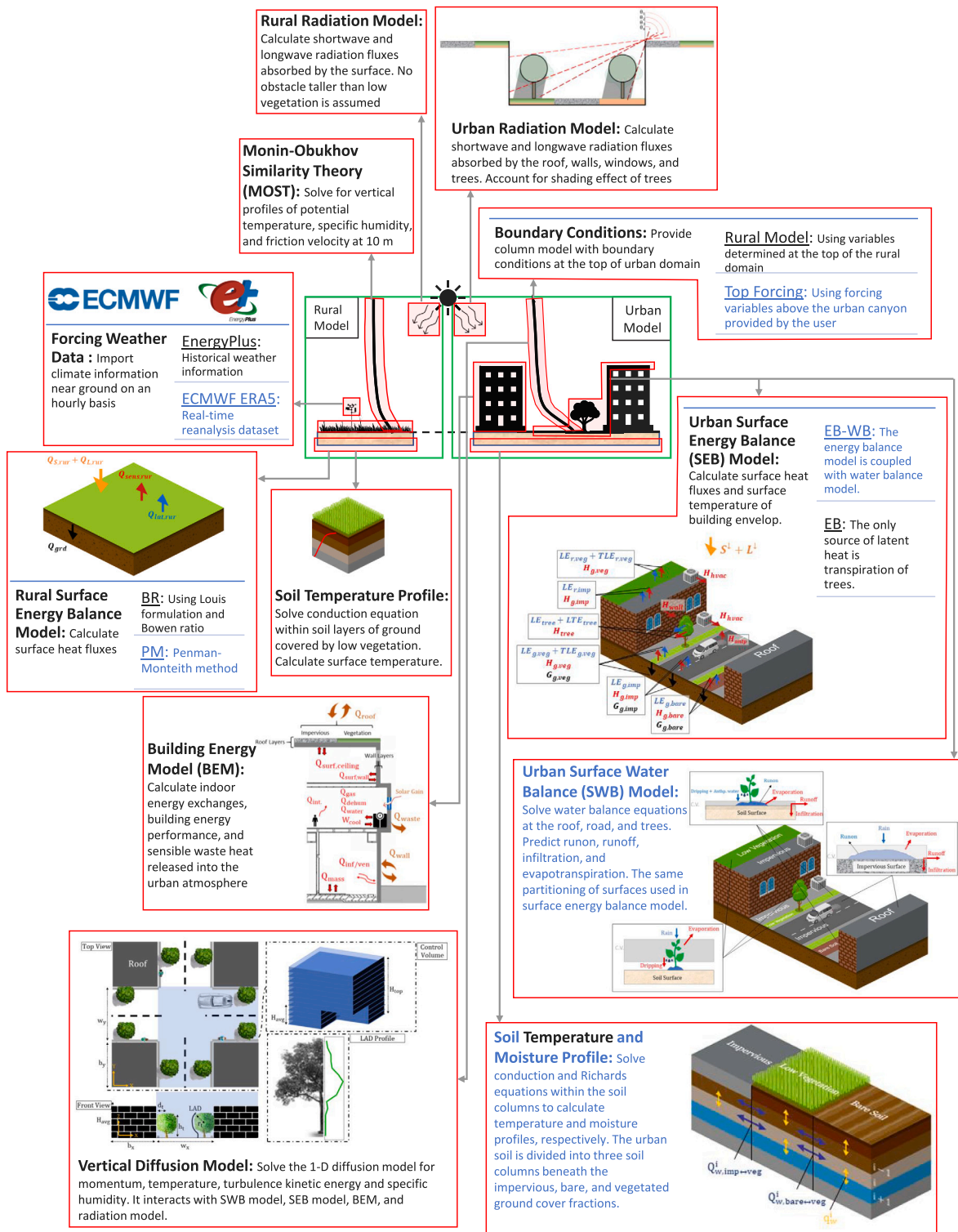
Fig. 1. Illustration of the Vertical City Weather Generator (VCWG v2.0.0) model and the constituent sub-models. The new modeling components in VCWG v2.0.0 (with respect to the predecessor model VCWG v1.3.2) are highlighted in blue. The rural model is furnished with the Penman–Monteith parameterization for surface energy balance. Alternative to the rural model, the forcing data can be retrieved from the ERA5 dataset and imposed on top of the urban model. The urban model is furnished with surface water balance and soil moisture parameterizations. (For interpretation of the references to color in this figure legend, the reader is referred to the web version of this article.)

2.2. Urban model

2.2.1. Radiation model

The radiation model calculates radiation fluxes on the urban surfaces after infinite reflections of longwave and shortwave rays within the urban canyon in the presence of trees, which is adopted from studies by Ryu et al. [59] and Meili et al. [50]. Presence of two trees is identified by geometric parameters including tree height h_t [m], crown radius r_t [m], distance from canyon walls d_t [m], and Leaf Area Index (LAI) [$m^2\ m^{-2}$], which is the vertical integral of the Leaf Area Density (LAD) [$m^2\ m^{-3}$].

The magnitude of direct shortwave radiation received by each urban surface element is computed by accounting for shade effects according to known methodologies for the case with no trees [14,15,45] and with trees [59]. Sky view factors determine the amount of diffuse shortwave radiation that arrives at a surface from the sky. Infinite reflections of diffuse shortwave radiation are computed within the urban canyon using view factors for each pair of urban surface elements [60,61]. These view factors are calculated analytically for the case with no trees [14,48,62]. If trees are considered, the view factors are computed with a basic two-dimensional Monte Carlo ray-tracing algorithm [61, 63]. More details about the radiation model are provided by Meili et al. [50] and Moradi et al. [51]. The absorbed (net) longwave radiation for each surface element is calculated as a function of surface temperature, surface emissivity, and the incident longwave radiation flux. Infinite reflections of longwave rays within the urban canyon are accounted for with the use of reciprocal view factors. More details about the radiation model are provided in the Appendix.

2.2.2. Surface energy balance model

The surface energy balance model parameterizes the exchange processes of heat between the atmospheric boundary layer and the urban surface elements. Due to the diversity of shape, size, and composition of urban surface elements, the surface energy balances in the urban areas are more difficult to model than the rural areas. Fig. 2 shows the energy fluxes from the urban surface elements. In VCWG, one can express the energy balance equation for the individual urban surface i as

$$L_{n,i} + S_{n,i} = H_i + LE_i + G_i, \qquad (3)$$

where the left hand side of the equation represents net allwave radiation fluxes at the surface element i (vegetated roof: (r,veg), impervious roof: (r,imp), vegetated ground: (g,veg), bare ground: (g,bare), impervious ground: (g,imp), wall, and tree), H_i [W m^{-2}] is sensible heat flux, LE_i [W m^{-2}] is latent heat flux, and G_i [W m^{-2}] is conductive heat flux. The latent heat flux at the walls are assumed to be zero. The sensible and latent heat fluxes can be calculated as [50]

$$H_i = -\rho C_{\mathrm{p}} \frac{\overline{\Theta}_{\mathrm{atm}} - \overline{\Theta}_i}{\sum_j r_{i,j}}, \qquad (4)$$

$$LE_i \text{ or } LTE_i = \rho L \frac{\overline{Q}_{\mathrm{sat}}(T_i) - \overline{Q}}{\sum_j r_{i,j}}, \qquad (5)$$

where ρ [kg m^{-3}] is density of air at the air temperature of $\overline{\Theta}_{\mathrm{atm}}$ [K] adjacent to the surface, L [J kg^{-1}] is the latent heat of vaporization, $\overline{Q}_{\mathrm{sat}}$ [kg kg^{-1}] is saturated specific humidity at the surface temperature T_i [K], $\overline{Q}$ [kg kg^{-1}] is the specific humidity of the adjacent air, and $\sum_j r_{i,j}$ [s m^{-1}] is the sum of thermal resistances between the surface and the atmosphere. VCWG accounts for aerodynamic, leaf boundary, soil, and stomatal resistances. Aerodynamic resistance for horizontal and vertical surfaces is calculated based on MOST and empirical convective heat transfer coefficients, respectively. The leaf boundary layer is a thin laminar layer of air surrounding the leaf, which controls the exchange of mass and energy between the plant and the surrounding environment. The leaf boundary resistance can be calculated as a function of leaf morphology and wind speed. Stomata of a leaf control the uptake of CO_2 from the atmosphere to its chloroplasts for photosynthesis activity. The stomatal resistance of sunlit and shaded vegetation are calculated separately. More details about the calculation of latent and sensible heat fluxes are provided in the Appendix and studies by Meili et al. [50] and Moradi et al. [51].

2.2.3. Urban hydrology model

Modeling of ecohydrological processes in natural areas has been undertaken for decades [64–67]. Recently, much attention has been also paid to such processes in the urban areas to support sustainable urban water management and to improve understanding of urban ecology. In this study, urban hydrological exchanges in the presence of precipitation and ecophysiological behavior of urban trees, road vegetation, and roof vegetation are modeled. The hydrology model solves the surface water balance equations for impervious surfaces, soil surfaces, and interception on urban vegetation, and it calculates transpiration as a function of soil moisture, photosynthetic activity, and vapor pressure deficit. The VCWG adopts the urban hydrology model developed by Meili et al. [50] with technical modifications that improve prediction of urban climate variables.

The transient equation for interception of water by urban vegetation (trees, roof, and road vegetation) and horizontal surfaces (impervious, bare soil, and soil underneath low vegetation) can be obtained as [50]

$$\frac{d\,Int}{dt} = P_{\mathrm{precip}} + P_{\mathrm{runon}} - D - E_{\mathrm{int}}, \qquad (6)$$

where Int [mm] is the intercepted water, P_{precip} [mm s^{-1}] is the fraction of total precipitation that reaches the surface, P_{runon} [mm s^{-1}] is runon, D [mm s^{-1}] is the water system outflow in forms of infiltration, deep leakage, and runoff, and E_{int} [mm s^{-1}] is the evaporation from intercepted water. It is assumed that the surface runoff and soil water leakage at the roof level travel directly to the sewer system and do not affect the water balance in the urban canyon.

Vertical and horizontal distribution of soil moisture in an urban area is one of the important preconditions for urban climate models. Soil moisture influences water and energy exchanges in the atmosphere and vadose (unsaturated) zone, which is defined as the part of earth spanning from land surface to the position at which the ground water is at atmospheric pressure. The vadose zone interacts with the active rooting zone and provides water needed for growth of vegetation, affects water balance at the surface by absorbing surface water and energy exchanges via changing latent heat flux, and controls the transmission of water from land surface to groundwater [68,69]. As shown in Fig. 3b, the vadose zone in an urban area is divided into the three soil columns underneath the vegetated, bare, and impervious surfaces. There is only one soil column at the roof level for green roofs. The first few layers of the soil column underneath the impervious surface do not contribute to water balance. The vertical water movement in the soil columns is modeled using the one-dimensional Richards equation, which is based on the ordinary laws of hydrodynamics and the driving mechanisms are gravity and the pressure gradient forces [50]. Then, the vertical Richards equation is coupled to the simplified horizontal equation, where the latter describes the dynamics of horizontal water flux for each layer

$$d_{z,i} \frac{d\theta_i}{dt} = (Q_{\mathrm{ver},i-1} - Q_{\mathrm{ver},i}) + (Q_{\mathrm{lat},i}^{\mathrm{in}} - Q_{\mathrm{lat},i}^{\mathrm{out}}) - \sum_{j=1}^{n_g} E_{\mathrm{soil},j}$$
$$- \sum_{j=1}^{n_g} T_{\mathrm{tree},j} \cdot r_{\mathrm{tree},i,j} - \sum_{j=1}^{n_g} T_{\mathrm{veg},j} \cdot r_{\mathrm{veg},i,j}, \qquad (7)$$

where $d_{z,i}$ [mm] is layer depth, θ_i [m^3 m^{-3}] is soil moisture content, $Q_{\mathrm{ver},i-1}$ and $Q_{\mathrm{ver},i}$ [mm s^{-1}] are the vertical water fluxes in and out of layer i, $Q_{\mathrm{lat},i}^{\mathrm{in}}$ and $Q_{\mathrm{lat},i}^{\mathrm{out}}$ [mm s^{-1}] are the lateral water fluxes in and out of the layer, and $E_{\mathrm{soil},j}$ [mm s^{-1}] is soil evaporation of surface j, which exists only in the first layer. In the presence of low vegetation and trees, the sink term due to the transpiration of low vegetation $T_{\mathrm{veg},j}$ [mm s^{-1}] and trees $T_{\mathrm{tree},j}$ [mm s^{-1}] from surface j should be taken into account. T_{veg} and T_{tree} [mm s^{-1}] are weighted based on the fraction of root biomass in the layer $r_{\mathrm{veg},i,j}$ [–] and $r_{\mathrm{tree},i,j}$ [–] of surface j. The low vegetation at the roof and ground levels can only access water stored in the soil column underneath the vegetated fraction of the surface. The horizontal distribution of the tree root can be set to either have access to all three soil columns or depending on the size of tree it can have access to a fraction of them [50].
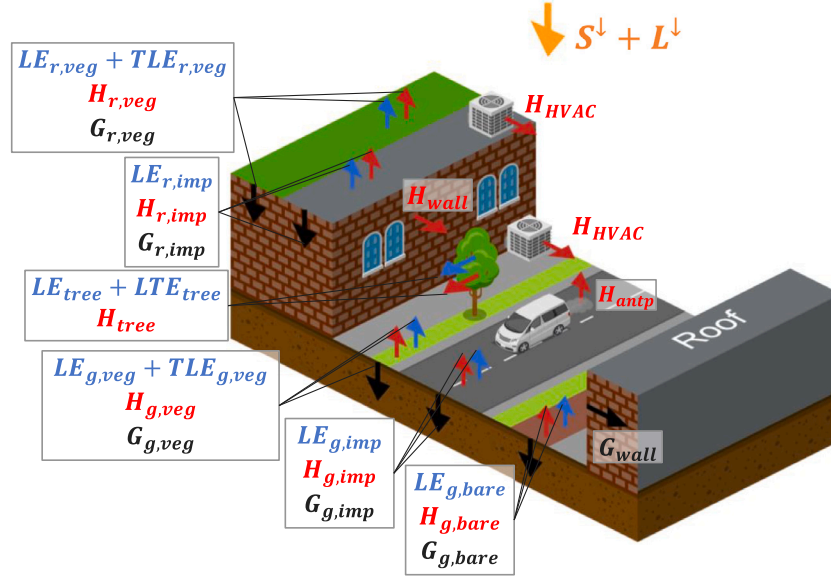
Fig. 2. Illustration of surface energy balance model in the urban area involving shortwave $S^{\downarrow}$, longwave $L^{\downarrow}$, sensible H_i, latent LE_i, evapotranspiration latent TLE_i, and ground G_i heat fluxes [W m^{-2}].
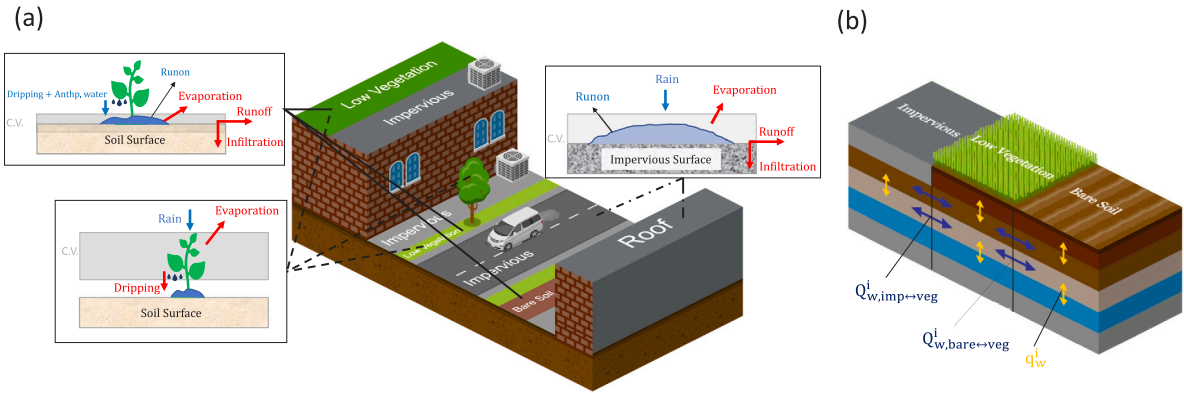

Fig. 3. Illustration of the (a) water balance model in the urban area and (b) partitioning of the soil column; the blue and red arrows are the source and sink terms, respectively, in the water balance equations; the black arrow is the indicator. (For interpretation of the references to color in this figure legend, the reader is referred to the web version of this article.)

2.2.4. Urban vertical diffusion model

VCWG utilizes a vertical diffusion model, which was originally developed by Santiago and Martilli [70], to calculate the vertical profiles of variables in the urban area including cross- and along-canyon wind velocity vector components, turbulence kinetic energy, potential temperature, and specific humidity. The source/sink terms in momentum and turbulence kinetic energy equations are parameterized based on CFD simulations. The sensible heat fluxes from ground (impervious, bare, and vegetated), walls, trees, roof (impervious and vegetated), building, and anthropogenic activities contribute to the sink/source terms in energy equation. The sources/sinks of specific humidity are contributed from the total latent heat fluxes from wet surfaces, trees, and vegetation at the ground and roof levels. The Appendix details the vertical diffusion equations.

2.2.5. Building energy model

The Building Energy Model (BEM) solves the sensible and latent heat balance at the indoor environment to determine the indoor temperature and humidity. The single thermal zone model calculates indoor air temperature and humidity with respect to the in-canyon averaged air temperature and specific humidity. The indoor energy balance accounts for the heat fluxes from building surfaces (wall, roof,

floor, windows, ceiling) Q_{surf} [W m^{-2}], internal heat sources $Q_{int,sens}$ [W m^{-2}], Heating Ventilation and Air Conditioning (HVAC) system $Q_{ven,sens}$ [W m^{-2}], and infiltration/exfiltration $Q_{inf,sens}$ [W m^{-2}], which can be formulated as

$$\forall \rho C_p \frac{dT_{in}}{dt} = \underbrace{\pm Q_{surf} \pm Q_{ven,sens} \pm Q_{inf,sens} \pm Q_{int,sens}}_{Q_{cool/heat}}, \quad (8)$$

where $\forall$ [m^3 m^{-2}] is indoor volume per building footprint area, T_{in} [K] is indoor air temperature, and $Q_{cool/heat}$ [W m^{-2}] is the building cooling or heating demand. In this notation all symbols represent positive quantities; however, in the equation either positive or negative signs should be used to emphasize if a term contributes to indoor temperature increase or decrease, depending on the operation mode (cooling versus heating) and environmental conditions (indoor, outdoor, and surface temperatures). Under cooling mode, the waste heat of the building ejected to the urban environment is calculated by $Q_{waste} = Q_{cool} + W_{cool}$ [W m^{-2}], where $W_{cool} = Q_{cool}/COP$ [W m^{-2}] is the energy consumption of the cooling system, which is determined by the Coefficient of Performance (COP) [–]. Under heating mode, the waste heat of the building ejected to the urban environment is calculated by $Q_{waste} = Q_{heat}/\eta_{heat} - Q_{heat}$ [W m^{-2}], where η_{heat} [–] is the thermal efficiency of the heating system.

Table 1

List of input parameters used in VCWG v2.0.0 for model evaluation in Basel and Vancouver; EB: Energy Balance, EB-WB: Energy Balance–Water Balance.

Parameter	Symbol	Vancouver	Basel
Latitude [°N]	lat	49.26	47.55
Longitude [°E]	lon	−123.13	7.58
Average buildings height [m]	H_{avg}	4.8	14.6
Width of canyon [m]	$w_x = w_y = w$	23	18.2
Building width to canyon width ratio [–]	$b_x/w_x = b_y/w_y = b/w$	0.4	1.1
Leaf Area Index [$m^2\ m^{-2}$]	LAI	0.39	0.41
Tree height [m]	h_t	5	8
Tree crown radius [m]	r_t	2	2.5
Tree distance from wall [m]	d_t	2.5	3
Building type	–	Mid-rise apartment	Mid-rise apartment
Urban albedos (roof, ground, wall, vegetation) [–]	$\alpha_R, \alpha_G, \alpha_W, \alpha_V$	0.13, 0.14, 0.2, 0.27	0.15,0.15,0.15,0.2
Urban emissivities (roof, ground, wall, vegetation) [–]	$\varepsilon_R, \varepsilon_G, \varepsilon_W, \varepsilon_V$	0.95,0.95,0.95,0.95	0.95,0.95,0.95,0.95
Ground aerodynamic roughness length [m]	z_{0G}	0.02	0.02
Roof aerodynamic roughness length [m]	z_{0R}	0.02	0.02
Ground fractions of vegetation, impervious, and soil coverage [–]	$f_{veg}, f_{imp}, f_{soil}$	0.5,0.5,0	0,1,0
Roof fractions of vegetation and impervious coverage [–]	f_{veg}, f_{imp}	0,1	0,1
Rural overall albedo [–]	α_{rur}	–	0.2
Rural overall emissivity [–]	ε_{rur}	–	0.95
Rural aerodynamic roughness length [m]	$z_{0,rur} = 0.1h_{rur}$	–	0.2
Rural roughness length for temperature [m]	$z_{\overline{\theta},rur} = 0.1z_{0,rur}$	–	0.02
Rural roughness length for specific humidity [m]	$z_{\overline{Q},rur} = 0.1z_{0,rur}$	–	0.02
Rural zero displacement height [m]	$d_{rur} = 0.5h_{rur}$	–	1
Rural Bowen ratio [–]	β_{rur}	–	0.9
Vertical resolution [m]	Δz	1	1
Time step [s]	Δt	60	60
Canyon axis orientation [°N]	θ_{can}	0	65
Urban boundary condition	–	Top forcing	Rural model
Urban surface energy balance model	–	EB-WB	EB

A similar approach is utilized to calculate indoor humidity, where latent heat fluxes are from dehumidification processes and internal sources, and the building dehumidification demand Q_{dehum} [W m^{-2}]. Full parameterization of these terms are provided in predecessor studies [22,27,51,71–75]

3. Results and discussion

In this section, first the VCWG v2.0.0 model results are evaluated against the micro-climate field measurements including the Basel UrBan Boundary Layer Experiment (BUBBLE) dataset in Basel, Switzerland, in 2002 [76,77] and the Sunset neighborhood field measurements conducted in Vancouver, Canada, in 2008 [78]. The simulation results are also compared with the predecessor version of VCWG v1.3.2 and other studies. Next, the model performance is explored by various parametric simulations related to seasonal variations, modification of ground vegetation, green and cool roofs, and changes in the Local Climate Zone (LCZ).

3.1. Model evaluation

3.1.1. Observation and forcing datasets

The model predictions of air temperature, wind speed, specific humidity, and sensible and latent heat fluxes are compared to the BUBBLE observations on an hourly basis. The BUBBLE field observation was conducted in an urban canyon (47.55°N and 7.58°E) with a canyon axis angle of $\theta_{can} = 65°$ and in a rural area approximately 7 km southeast of Basel. Wind speed and potential temperature were measured at six levels in the urban site from near ground to a height above canyon. Specific humidity was measured at two levels in and above the canyon. The rural measurements were formatted as an EPW file to force the model. For details of this campaign see the studies by Christen and Vogt [76] and Moradi et al. [51].

Measurements in the Sunset neighborhood of Vancouver (49.26°N and −123.13°E) consisted of air temperature and relative humidity at 26 m a.g.l, incoming shortwave and longwave radiation fluxes at 26.2 m a.g.l, and barometric pressure, latent, and sensible heat fluxes at 28.8 m a.g.l. The dataset provides the measurements averaged every

Table 2

Bias, RMSE, and R^2 for VCWG v1.3.2 and VCWG v2.0.0 predictions of potential temperature $\overline{\Theta}$ [K], wind speed $\overline{S}$ [m s^{-1}], and specific humidity $\overline{Q}$ [kg kg^{-1}] against the BUBBLE observations averaged over all altitudes.

Statistic	VCWG v1.3.2			VCWG v2.0.0			Difference		
	$\overline{\Theta}$	$\overline{S}$	$\overline{Q}$	$\overline{\Theta}$	$\overline{S}$	$\overline{Q}$	$\overline{\Theta}$	$\overline{S}$	$\overline{Q}$
Bias	−0.31	0.9	0.00065	−0.53	−0.46	0.0000	–	–	–
RMSE	1.06	0.96	0.0013	0.56	0.44	0.0003	0.5	0.52	0.001
R^2	0.93	0.42	0.42	0.98	0.46	0.98	0.05	0.04	0.56

5 min. The urban canyon axis is oriented in the north direction with canyon axis angle of $\theta_{can} = 0°$. The measured downwelling shortwave and longwave radiation fluxes, air temperature, humidity, and pressure are used to force the model at the top of the simulation domain. The model predictions of sensible and latent heat fluxes are compared to the observations on an hourly basis.

The input parameters representing the urban area in Basel and Vancouver are listed in Table 1. The input parameters are inferred from variables, datasets, and simulation codes in the literature that pertain to the field campaigns and associated models as well as general assumptions found in the literature [22,30,59,76,78]. For the Basel case, the simulations are conducted for 15 days with one day of spin-up period starting from June 15, 2002, which is consistent with other studies [59,79,80]. For the Vancouver case, the simulations are conducted for five months from May 2008 to September 2008 with one day of spin-up period. The simulation time step for both analyses is 1 min. Ideally longer spin up times would be desirable for establishment of model internal variables that have a long response time to environmental conditions, such as the soil moisture levels.

3.1.2. Potential temperature, wind speed, and specific humidity

To compare VCWG v2.0.0 results with measured meteorological variables from the BUBBLE campaign, the Bias, Root Mean Square Error (RMSE), and coefficient of determination R^2 are computed for pairs of model versus observed values every hour for available altitudes. This analysis is performed for wind speed, potential temperature, and specific humidity. The results from VCWG v1.3.2 and VCWG v2.0.0 are

provided in Table 2. Considering all altitudes, the average Bias, RMSE, and R^2 for potential temperature are −0.53 [K], 0.56 [K], and 0.98 [−], which are improved in comparison to the predecessor version of the model. Considering all altitudes, VCWG v2.0.0 simulation results show improvement in RMSE and R^2 for potential temperature, as the RMSE is decreased by 0.5 [K] and R^2 is increased by 0.05 [−]. The average Bias, RMSE, and R^2 for wind speed are −0.46 [m s^{-1}], 0.44 [m s^{-1}], and 0.46 [−], which are improved in comparison to the predecessor version of the model. Considering all altitudes, VCWG v2.0.0 simulation results show improvement in RMSE and R^2 for wind speed, as the RMSE is decreased by 0.52 [m s^{-1}] and R^2 is increased by 0.04 [−]. VCWG v2.0.0 also shows better performance in estimating the specific humidity within and above the canyon. The average Bias, RMSE, and R^2 for specific humidity are 0.000 [kg kg^{-1}], 0.0003 [kg kg^{-1}], and 0.98 [−], respectively. Considering all altitudes, VCWG v2.0.0 simulation results show improvement in RMSE and R^2 for specific humidity, as the RMSE is decreased by 0.001 [kg kg^{-1}] and R^2 is increased by 0.56 [−]. Such improvement is mainly attributed to incorporation of the hydrology model and more accurate representation of the sources and sinks for the latent heat flux in the urban vertical diffusion model.

3.1.3. Sensible and latent heat fluxes

The VCWG v2.0.0 is further assessed based on the comparison between the measured and simulated urban sensible H_{urban} [W m^{-2}] and urban latent LE_{urban} [W m^{-2}] heat fluxes above the canyon. H_{urban} and LE_{urban} are calculated as functions of potential temperature and specific humidity gradients, respectively, obtained from the urban vertical diffusion model and turbulent diffusion coefficient (K_m [m^2 s^{-1}])

$$H_{\mathrm{urban}} = -\left(\rho C_p \frac{K_m}{Pr_t} \frac{\partial \overline{\Theta}}{\partial z} \right)_{z=z_{\mathrm{obs}}} \tag{9}$$

$$LE_{\mathrm{urban}} = -\left(\rho L \frac{K_m}{Sc_t} \frac{\partial \overline{Q}}{\partial z} \right)_{z=z_{\mathrm{obs}}}, \tag{10}$$

where z_{obs} [m] is the height at which sensible/latent heat fluxes are measured, and Pr_t and Sc_t [−] are the turbulent Prandtl and Schmidt numbers, respectively [81], with values provided by Moradi et al. [51]. For the Basel case, the heat fluxes are measured at the altitude of 31.7 [m] above ground. The statistical analysis provided in Table 3 shows that VCWG v2.0.0 results in a lower Bias, lower RMSE, and higher R^2 relative to the results from VCWG v1.3.2. VCWG v2.0.0 results in Bias, RMSE, and R^2 of 22 [W m^{-2}], 34.3 [W m^{-2}], and 0.88 [−], respectively, for sensible heat flux and −17.3 [W m^{-2}], 23.1 [W m^{-2}], and 0.35 [−], respectively, for latent heat flux. Considering the short evaluation period using VCWG v2.0.0, the model shows reasonable performance in comparison to the previous studies that reported Bias of −4.15 [W m^{-2}] [59] and −71.8 [W m^{-2}] [82] and RMSE of 38.9 [W m^{-2}] [59] and 100.2 [W m^{-2}] [82] for sensible heat flux and Bias of −20.6 [W m^{-2}] [59] and RMSE of 33.8 [W m^{-2}] [59] and 36.0 [W m^{-2}] [82] for latent heat flux.

The capability of VCWG v2.0.0 to predict latent and sensible heat fluxes over longer periods of time is evaluated against the Vancouver Sunset dataset. For this analysis, the model is forced at the top of the urban domain using the observed dataset over five months. Fig. 4 illustrates the cross-comparison between VCWG v2.0.0 simulation results and the field measurements. The simulated and observed urban sensible heat flux show reasonable agreement with a Bias, RMSE, and R^2 of 0.65 [W m^{-2}], 18.1 [W m^{-2}], and 0.94 [−], respectively (see Table 3). Compared to the previous studies, Oleson et al. [83] obtained Bias of 62 [W m^{-2}], RMSE of 81 [W m^{-2}], and R^2 of 0.87 [−] using an urban parameterization for a global climate model. The results from the Surface Urban Energy and Water balance Scheme (SUEWS) model showed RMSE of 39.1 [W m^{-2}] and R^2 of 0.77 [−] [46]. This comparison signifies the adequate performance of VCWG v2.0.0. Urban latent heat flux is also well-captured with the model. The statistics show

that VCWG v2.0.0 simulated LE_{urban} with a Bias, RMSE, and R^2 of 1.35 [W m^{-2}], 27.7 [W m^{-2}], and 0.55 [−], respectively, compared to the other studies that reported Bias of −4 [W m^{-2}] [83], 1.9 [W m^{-2}] [50], RMSE of 16 [W m^{-2}] [83], 32.5 [W m^{-2}] [46], 26.8 [W m^{-2}] [50], and R^2 of 0.35 [−] [83], 0.74 [−] [46], and 0.62 [−] [50]. This demonstrates the reasonable performance of VCWG v2.0.0 relative to observations and previous studies.

3.2. Model exploration

The performance of VCWG v2.0.0 is assessed by evaluating the model for different seasons, coverages of urban trees and ground vegetation, roof types (green and cool roofs), and Local Climate Zones (LCZs). All explorations are performed by VCWG v2.0.0 simulations of the urban micro-climate variables in Vancouver, Canada. For the seasonal and roof type analyses, the model is automated to run for a whole year in 2007. The other analyses are conducted in a warm month (July). The spatial distribution of climate variables is simulated by coupling an automated GIS process function with VCWG v2.0.0. For these analyses, the ERA5 dataset is used to force the model at the top of the urban domain at an elevation of 90 m above ground, which is higher than the urban roughness layer, typically 2–5 times of the building height [84]. The input parameters representing the urban area and the model options used for these explorations are listed in Table 4. Depending on the type of analysis, the input parameters vary within an appropriate range that are discussed in the subsequent sections.

3.2.1. Seasonal variations

Compared to the regions close to the equator, the areas at higher latitudes (greater than 45 degrees) experience stronger seasonal variability in the cycle of surface energy and water fluxes [85]. The amount of solar radiation flux reaching the Earth's surface and the solar zenith angle vary significantly over the course of a year, leading to different meteorological conditions, shading effects, foliage amounts, soil moisture content, patterns of anthropogenic heat fluxes, and building energy performance.

As shown in Fig. 5, the urban area is characterized by higher latent and sensible heat fluxes in the warm season (April–September). While the sensible and latent heat fluxes follow approximately the same trend and magnitude during the cold season (January–March and October–December), the sensible heat flux is substantially higher during the summer months. Although the sensible heat flux in cold months is considerably lower, it still transfers energy from surfaces to the urban boundary layer with a daytime mean value of 60 [W m^{-2}]. This suggests that the building waste heat and other anthropogenic activities in the urban areas are dominant during cold months (see Fig. 7). The larger values of heat fluxes in the summer months is mainly attributed to the larger magnitude of solar radiation fluxes interacting with the urban surfaces and the growth of active vegetation. The latent heat flux is mainly characterized by the moisture availability in the urban area. Due to the high impervious surface coverage in the urban area, the latent heat flux exhibits less seasonal variation. However, more active vegetation in the warm months contributes significantly to the total latent heat flux and increases the daytime mean value of latent heat flux from 50 [W m^{-2}] in the winter to 90 [W m^{-2}] in the summer. In other words, the higher net radiation in the warm months leads to a higher vapor pressure deficit. However, this analysis is a strong function of climate zone. For instance, tropical regions (e.g. Singapore) experience less variability in latent heat flux with fluctuations around 80 [W m^{-2}] [50]. On the other hand, regions at higher latitudes show more variability, which is consistent with the findings in this study (e.g. Melbourne: latent heat flux from 40 [W m^{-2}] in the winter to 140 [W m^{-2}] in the summer [50,85]; London: latent heat flux from 20 [W m^{-2}] in the winter to 80 [W m^{-2}] in the summer [86]). Precipitation and anthropocentric water (e.g. irrigation) are the main contributors to the latent heat flux in the urban areas. Prescribed time
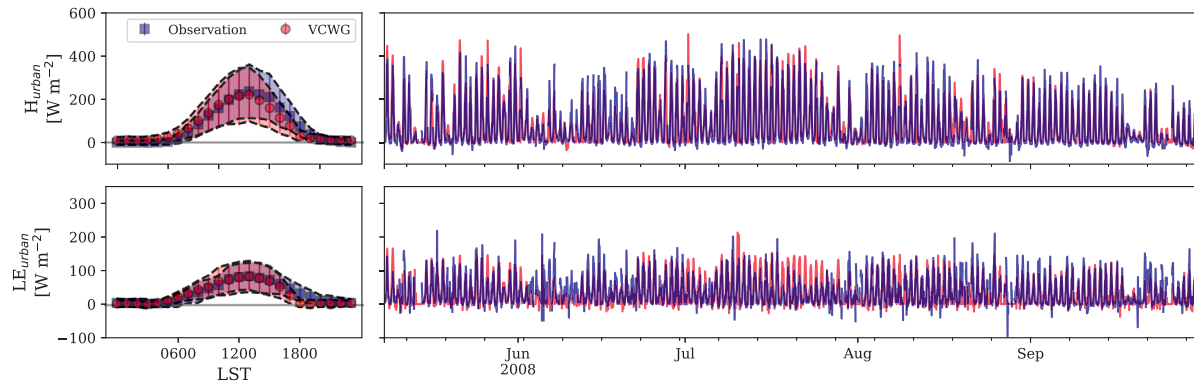
Fig. 4. Comparison between the Vancouver Sunset dataset (blue/squares) versus simulated (red/circles) values of sensible and latent heat fluxes above the urban area using VCWG v2.0.0; the hourly means are shown; times in Local Standard Time (LST); simulation for a 5-month period in 2008. The shaded area is sensible/latent heat flux ± standard deviation. (For interpretation of the references to color in this figure legend, the reader is referred to the web version of this article.)

Table 3

Bias, RMSE, and R^2 for VCWG predictions of sensible and latent heat fluxes [W m^{-2}] against the observations and previous studies.

Urban fluxes	VCWG v1.3.2			VCWG v2.0.0			Literature		
	Bias	RMSE	R^2	Bias	RMSE	R^2	Bias	RMSE	R^2
H_{urban}(Vancouver)	–	–	–	0.65	18.1	0.94	62[a]	81[a],39.1[c]	0.87[a],0.77[c]
H_{urban}(Basel)	−45.2	63.5	0.58	22.0	34.3	0.88	−4.15[b],−71.8[d]	38.9[b],100.2[d]	–
LE_{urban}(Vancouver)	–	–	–	1.35	27.7	0.55	−4[a]	16[a],32.5[c]	0.35[a],0.74[c]
LE_{urban}(Basel)	−28.7	37.1	0.28	−17.3	23.1	0.35	−20.6[b]	33.8[b],36.0[d]	–

[a]Oleson et al. [83] evaluation period is 15 days.

[b]Ryu et al. [59] evaluation period is 30 days.

[c]Järvi et al. [46] evaluation period is 147 days.

[d]Kawai et al. [82] evaluation period is 39 days.

Table 4

List of input parameters used in VCWG v2.0.0 for model explorations in Vancouver.

Parameter	Symbol	Value
Latitude [°N]	lat	49.23
Longitude [°E]	lon	−123.08
Average buildings height [m]	H_{avg}	10.0
Width of canyon [m]	$w_x = w_y = w$	23.0
Building width to canyon width ratio [–]	$b_x/w_x = b_y/w_y = b/w$	0.4
Tree height [m]	h_t	8.0
Tree crown radius [m]	r_t	1.5
Tree distance from wall [m]	d_t	2.2
Leaf area index [m^2 m^{-2}]	LAI	Variable
Building type	–	Mid-rise apartment
Urban albedos (roof, ground, wall, vegetation) [–]	$\alpha_R, \alpha_G, \alpha_W, \alpha_V$	0.13, 0.14, 0.2, 0.27
Urban emissivities (roof, ground, wall, vegetation) [–]	$\varepsilon_R, \varepsilon_G, \varepsilon_W, \varepsilon_V$	0.95, 0.95, 0.95, 0.95
Ground fractions of vegetation, impervious, and soil coverage [–]	$f_{veg}, f_{imp}, f_{soil}$	Variable
Roof fractions of vegetation and impervious coverage [–]	f_{veg}, f_{imp}	Variable
Vertical resolution [m]	Δz	1
Time step [s]	Δt	300
Canyon axis orientation [°N]	θ_{can}	0.0
Urban boundary condition	–	Top forcing
Urban surface energy balance model	–	EB-WB

series of anthropocentric water for vegetated and bare surfaces can be considered in the simulation. Days with more precipitation, particularly in the warm months, are more likely to have increased latent heat flux and decreased sensible heat flux (e.g. late August and early September in Fig. 5). The results obtained from this exploration are in reasonable agreement with other studies [50,85,86].

Due to the high variability of radiative, thermal, and moisture properties of the urban surfaces, they more likely experience different temperatures through a diurnal cycle. The surface temperature controls the magnitude and direction of heat fluxes at the surface. Fig. 6 shows the daytime and nighttime percentiles of urban surface temperatures in January, May, August, and November, which are indicative of each season. Diurnal variation of the roof temperature is considerably higher

than the other surfaces, as roofs are directly exposed to solar radiation fluxes and are less influenced by the in-canyon surfaces [21]. In the warm months (May and August), all surfaces experience higher temperatures than the canyon air temperature except ground vegetation that remains close to the air temperature. During nighttime, there is a substantial decrease in roof temperature, while building walls have the highest temperatures, and temperature of vegetation remains close to the air temperature. The same pattern was observed by Christen et al. [87] and Aliabadi et al. [21], where roof and lawn temperatures fell below the canyon air temperature during the nighttime. In general, surfaces with higher temperature fluctuations (roof) exhibit considerably higher daytime temperatures than the canyon air temperature, which is consistent with the findings in the literature [21,87,88]. This analysis signifies the effect of replacing natural areas by impervious surfaces.
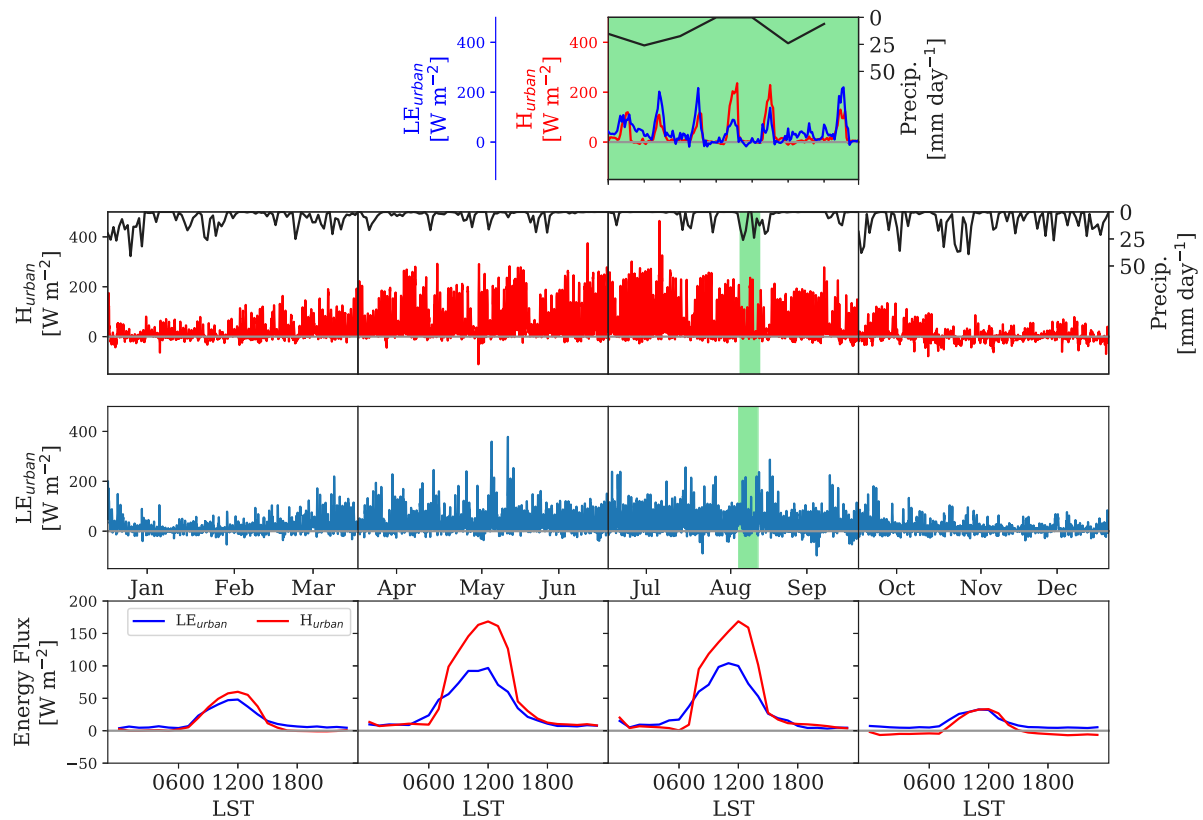
Fig. 5. Hourly simulated sensible and latent heat fluxes [W m^{-2}] for Vancouver in 2007; (top) sensible heat flux above the canyon over the course of a year; (middle) latent heat flux above the canyon over the course of a year; (bottom) mean diurnal variation of latent (blue) and sensible (red) heat fluxes for January–March, April–June, July–September, and October–December; (inset) a period of seven days is highlighted. The black line shows daily precipitation [mm day^{-1}]. (For interpretation of the references to color in this figure legend, the reader is referred to the web version of this article.)
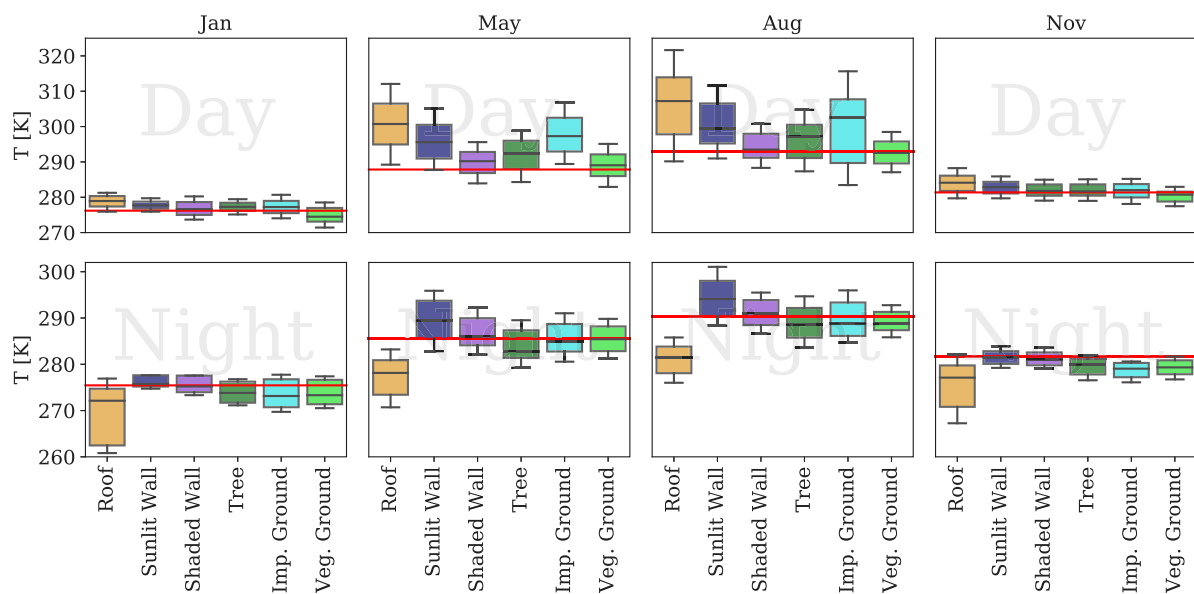
Fig. 6. Variability of urban surface temperatures in January, May, August, and November for Vancouver in 2007; the roof is impervious and the ground is partially covered by vegetation; the box plot represents 5th, 25th, 50th, 75th, and 95th percentiles for temperature; red line is canyon median air temperature; top row is the daytime and bottom row is the nighttime; daytime temperatures are sampled from 1000 to 1400 LST, and nighttime temperatures are sampled from 2200 to 0200 LST.

Building waste heat released into the atmosphere is considered as the main source of anthropogenic heat in the urban areas and is controlled by the building heating and cooling demand [89]. In cold months, when the building energy system is on heating mode, the building heat emission dominates the urban sensible heat flux and can

alter the urban air temperatures [90]. Fig. 7 shows the total building energy fluxes for three-month periods of the year. The heating and cooling demands are at their maximum in the cold months and the warm month, respectively. Shoulder seasons are the transition period from cooling (heating) mode to heating (cooling) mode, for fall (spring). A
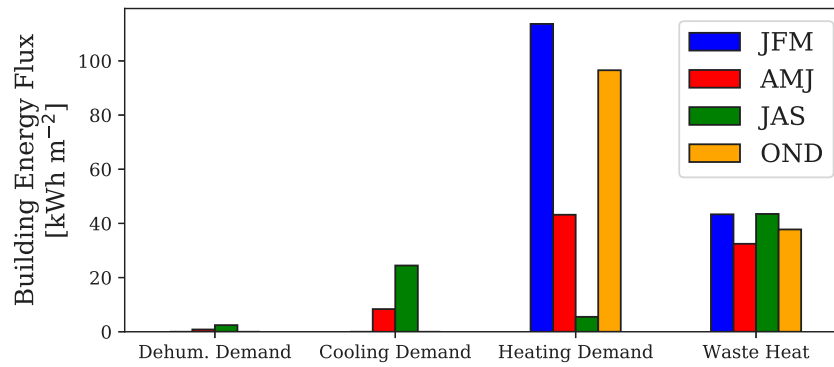
Fig. 7. Seasonal variation of the total building energy fluxes integrated over a three-month period including cooling demand (Q_{cool}), dehumidification demand (Q_{dehum}) heating demand (Q_{heat}), and building waste heat (Q_{waste}) within JFM (January, February, and March), AMJ (April, May, and June), JAS (July, August, and September), and OND (October, November, and December) months. The simulation is conducted for Vancouver in 2007.
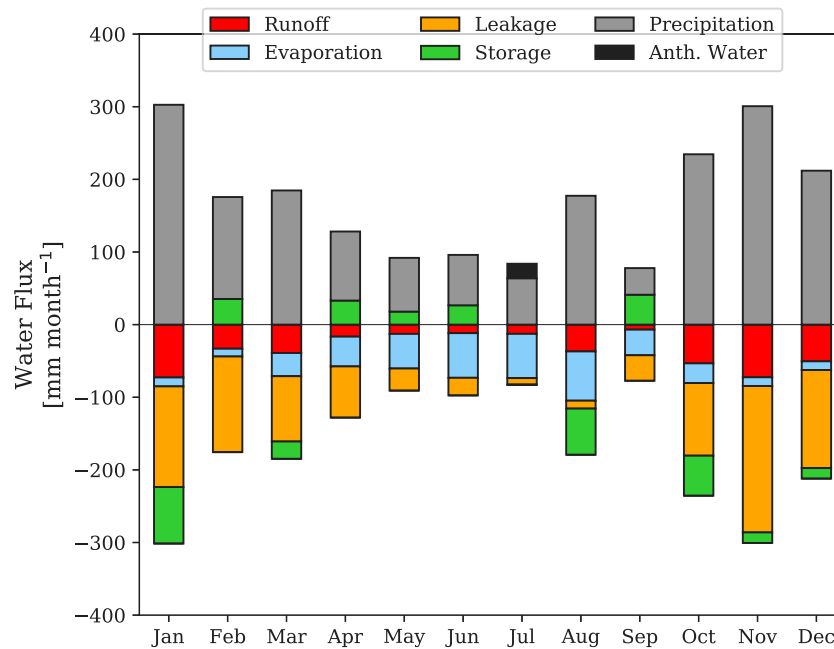

Fig. 8. Monthly variation of water balance components for Vancouver in 2007; hourly terms in the water balance equation are integrated over time to calculate the monthly magnitude for all sink, source, and storage terms.

small amount of energy is required for dehumidification in the warm months.

Water budget analysis in urban areas is mostly carried out on a seasonal or annual basis, which provides insight into the urban water management to cope with extreme weather conditions [91]. In an urban unit the precipitation and anthropogenic water (e.g. garden irrigation) are the main water inputs to the urban hydrologic cycle that are partitioned into surface runoff, evaporation, leakage at the bottom of the soil column, and depression storage [91,92]. Performance of VCWG to take into account the seasonal variation of water budget terms is assessed. Fig. 8 depicts the monthly variation of water balance terms for an entire year in Vancouver. In warm months, a large fraction of input water (precipitation plus anthropogenic water) is returned to the atmosphere via evaporation in forms of evapotranspiration, soil evaporation, and intercepted water evaporation. Due to the replacement of natural areas by impervious surfaces in the urban areas, a considerable fraction of precipitations moves over land. This surface runoff is higher during cold seasons, when cold weather restricts water evaporation. Urban runoff usually hits a peak during and immediately after rainfall events. In general, the ratio of surface runoff to precipitation varies from 0.3 in the winter to 0.1 in the summer. The same pattern has been

observed in the Oakridge, Vancouver, suburban area in 1982, where maximum evaporation and surface runoff were reported in June and January, respectively [93]. During the warm months, particularly in July, rainfall is reduced significantly and urban vegetation and soil are the main sources for water evaporation. This period of the year experiences extensive soil moisture depletion; water storage in the urban unit is approximately zero; and leakage is at its minimum. Extreme precipitation events, which usually occur in cold months in Vancouver, replenish the soil column, increase the soil moisture content, and may surpass the maximum capacity of the soil.

3.2.2. Effect of low vegetation on runoff and evaporation

Vegetation can alter the energy and water balance in the urban area and ultimately mitigate the negative impacts of UHI and urban flooding during extreme weather events. The effect of low vegetation on water budget terms are assessed for Vancouver in the summer. For this exploration, the model input variables are listed in Table 4. Urban vegetation has the desired effect of reducing flood hazards in the urban area. As shown in Fig. 9, increasing the low vegetation coverage fraction f_{veg} from 0 to 1 can substantially decrease the surface runoff from 1.7 [mm day^{-1}] to almost zero, while evaporation flux and deep
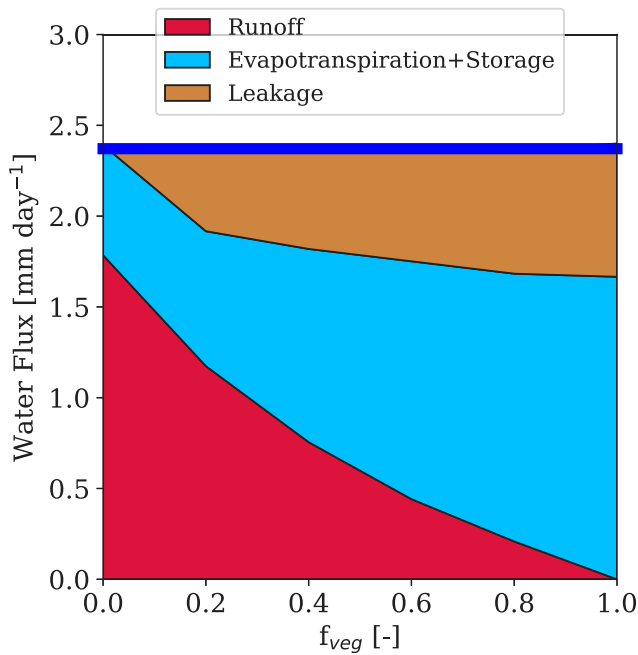
Fig. 9. Effect of low vegetation coverage fraction f_{veg} on mean daily water budget terms [mm day^{-1}] for Vancouver in July 2007; storage term is not significant, so it is added to the evaporation term; f_{veg} varies from 0 (road is all covered by impervious surface) to 1 (road is all covered by vegetation); the blue line is the mean daily rainfall [mm day^{-1}]. (For interpretation of the references to color in this figure legend, the reader is referred to the web version of this article.)

leakage increase. The results from this exploration are consistent with the simulation results from the UT&C model, where increasing f_{veg} from 0 to 1 for a case study in Singapore resulted in reduction of surface runoff from 4.5 [mm day^{-1}] to zero with a mean daily rainfall of 5 [mm day^{-1}] [50].

3.2.3. Effect of Green and cool roofs on model output variables

Given the growing demand for energy in urban areas, numerous energy saving technologies have been employed to mitigate the environmental effects of buildings and improve building energy performance. Green and cool roofs are common technologies for reducing heat in urban areas, building energy demand, and moderating roof and canyon surface temperatures. He et al. [94] simulated the performance of a building with green roof in Shanghai and showed that this technology can save cooling energy demand by 6.2%. Cool roofs with radiative properties of high solar albedo and high thermal emissivity, reduce urban heat, surface temperature, and improve building energy performance. Such an urban environment regulation is accomplished by reflecting more solar radiation fluxes and absorbing less heat, compared to the standard roofs [95,96]. Simulation results obtained from integrating BEP-BEM into WRF in a semi-arid urban environment (Phoenix and Tucson) showed that cool roofs can reduce cooling energy demand by 14% [97]. Krayenhoff et al. [98] showed that cool roofs provide about 0.2–0.6 [K] of cooling per 0.1 neighborhood albedo increase.

The effects of green and cool roofs on urban heat mitigation, roof surface temperature, and building energy performance are studied by simulating VCWG for an entire year in Vancouver in 2007. For the base case simulation, the roof surface is all covered by impervious surface ($f_{veg} = 0$ [–]) and the radiative properties are as listed in Table 4. For the green roof scenario, half of the roof surface is covered by low vegetation ($f_{veg} = 0.5$ [–]) with leaf area index (LAI) of 2.5 [m^2 m^{-2}] and soil layer thickness of 100 [mm]. No lateral water flux is calculated for the soil column, as there is only one soil column underneath the vegetated surface. Roof soil is composed of 0.2, 0.4, and 0.025 fraction

of clay, sand, and organic material, respectively. An exponential root profile is considered as the root biomass profile. To investigate the environmental effect of a cool roof, the surface albedo is increased to 0.7 [–], which is common for roofs coating with high reflective material [94].

Cool roofs can decrease the daytime roof surface temperatures by 10 [K] in the summer with no change on nighttime surface temperatures, as expected (see Fig. 10). While green roofs reduce surface temperatures to a lesser extent than cool roofs, they can decrease temperature fluctuations more effectively, particularly in warm months. Plant type, fraction of roof vegetation coverage, and soil properties control the green roof performance. Green and cool roofs can also increase the thermal comfort at the street level by reducing air temperature. Fig. 11 shows the cooling effect of green and cool roofs on canyon air temperature, which is more significant during warm months. It is worth noting that cool roofs can reduce canyon air temperature more effectively than green roofs. In terms of annual building energy performance, buildings with cool roofs save 16.1% cooling energy demand and 16.0% dehumidification energy demand. However, buildings with green roofs are less efficient and only save 5.2% cooling energy demand and 5.0% dehumidification energy demand. Fig. 12 illustrates the maximum building energy loads and sensible waste heat from buildings to the atmosphere for different seasons. It is worth noting that these technologies work more effectively in the warm months as they can increase the heating demand during the cold months due to their cooling effects, which can be observed from this analysis. Additionally, green and cool roofs reduce the annual building waste heat by 4% and 1%, respectively. This analysis shows that VCWG can adequately predict impacts of green and cool roofs on both buildings and outdoor climate.

3.2.4. Variation of local climate zone and model output variables

Local urban climate is primarily influenced by urban morphometric variables such as building plan area density, frontal area density, anthropogenic activities, and urban vegetation. There could be some pre-defined diurnal/seasonal schedule for human activities, however some other factors such as urban morphometric variables could vary over a longer time scale. One may experience different climate conditions within a city and one may sense such changes by traveling from the high-density built-up regions to the areas with more open space and ultimately rural areas. Stewart and Oke [99] developed the Local Climate Zone (LCZ) classification that identifies a region based on its ability to modify local surface climates. The surface thermal properties, land cover, and land structure define LCZ 1 as compact highrise to LCZ 9 as sparsely built areas. In this classification LCZ 10 is considered as an area with heavy industrial activities and LCZs A to G represent natural areas, which are out of scope of this study (For further details, readers are referred to Stewart and Oke [99]).

In this section, the capability of VCWG to simulate climate variables within the urban roughness sublayer for a typical city is investigated. It is assumed that the urban area is extended from LCZ 1 at the center to LCZ 9 far from the center. Fig. 13 shows the spatial variation of plan area density (λ_p [–]), leaf area index of urban trees (LAI_{tree} [m^2 m^{-2}]), canyon aspect ratio (H/W [–]), and fraction of ground covered by vegetation (f_{veg} [–]). The building area density and canyon aspect ratio vary from 0.6 to 0.2 [–] and 3.0 to 0.2 [–], respectively. Such a setup alongside with the urban trees are accompanied with ground–sky view factor variations from 0.15 [–] in the compact highrise region to 0.9 [–] in the sparsely built region. The range of variation of these parameters are consistent with the typical properties that are considered for LCZ 1 to LCZ 9 [99]. More high and low vegetation covers are considered as moving away from high-density built-up areas by changing f_{veg} (ground) and LAI_{tree} from 0.1 to 0.85 [–] and 1 to 4 [m^2 m^{-2}], respectively.

It has been observed that nocturnal UHI increases as urban heat flux increases and wind speed decreases [1,100]. As shown in Fig. 15,
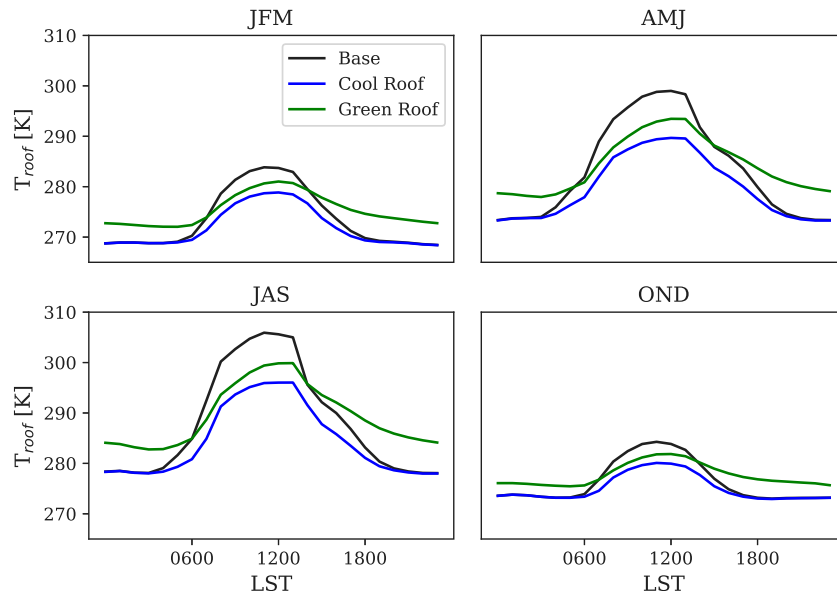
Fig. 10. Effects of green and cool roofs on roof surface temperature [K] in different seasons; the surface temperatures are diurnally-averaged over January–February–March (JFM), April–May–June (AMJ), July–August–September (JAS), and October–November–December (OND) for Vancouver in 2007. (For interpretation of the references to color in this figure legend, the reader is referred to the web version of this article.)
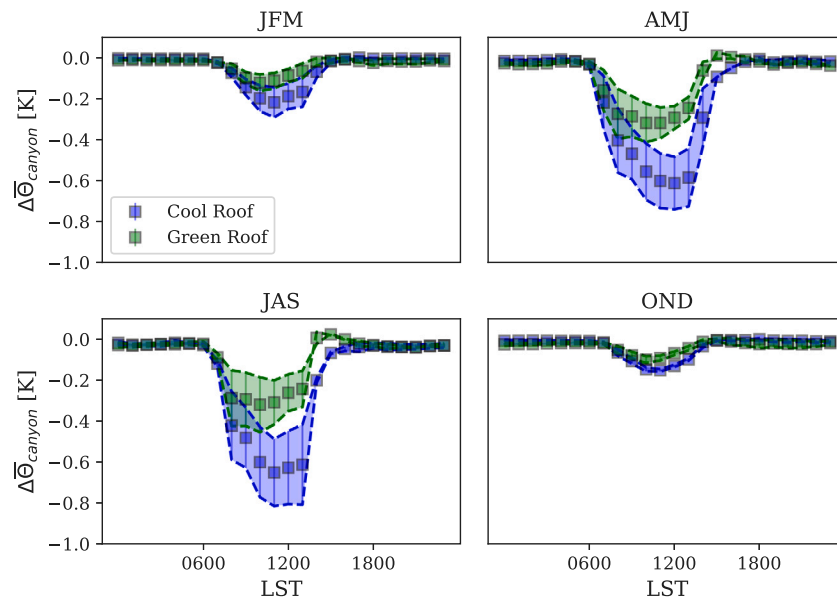

Fig. 11. Effects of green and cool roofs on canyon air temperature [K] in different seasons; hourly mean and standard deviation of the canyon air temperature difference between the base case and green roof ($\Delta\overline{\Theta}_{canyon} = \overline{\Theta}_{canyon}^{base} - \overline{\Theta}_{canyon}^{GR}$) and the canyon air temperature difference between the base case and cool roof ($\Delta\overline{\Theta}_{canyon} = \overline{\Theta}_{canyon}^{base} - \overline{\Theta}_{canyon}^{CR}$) are calculated over January–February–March (JFM), April–May–June (AMJ), July–August–September (JAS), and October–November–December (OND) for Vancouver in 2007. (For interpretation of the references to color in this figure legend, the reader is referred to the web version of this article.)

built-up areas slow down the wind speed within the canyon and consequently reduce turbulent mixing. Lower magnitude of forcing wind speed during nighttime facilitates trapping of heat within the canyon and increasing air temperatures. Figs. 14 and 16 show larger magnitudes of air temperatures and sensible heat fluxes in the compact high-rise region, respectively. Thus, higher temperature in high-density built-up areas than the surrounding sub-urban and rural areas can lead to nocturnal UHI. For the daytime, areas with higher canyon aspect ratio (H/W [–]) trap building released waste heat, which can lead to higher surface and air temperatures and urban sensible heat fluxes (see Figs. 14 and 16). As discussed earlier, urban vegetation can significantly cool down urban environments. Increasing urban vegetation as moving away from the urban center can increase latent heat fluxes by

100 [W m^{-2}], particularly during daytime (see Fig. 16). This process is accompanied with lowering sensible heat fluxes by 150 [W m^{-2}] and canyon air temperatures by 3 [K], as shown in Figs. 14 and 16, respectively.

4. Conclusions

The Vertical City Weather Generator (VCWG v2.0.0) is a computationally-efficient and operationally-simple urban micro-climate model, which considers the effects of urban vegetation, urban hydrology, building energy, and the connection to the surrounding rural area. VCWG v2.0.0 is a refinement of an earlier version, VCWG v1.3.2 [51]. While the performance of VCWG v1.3.2
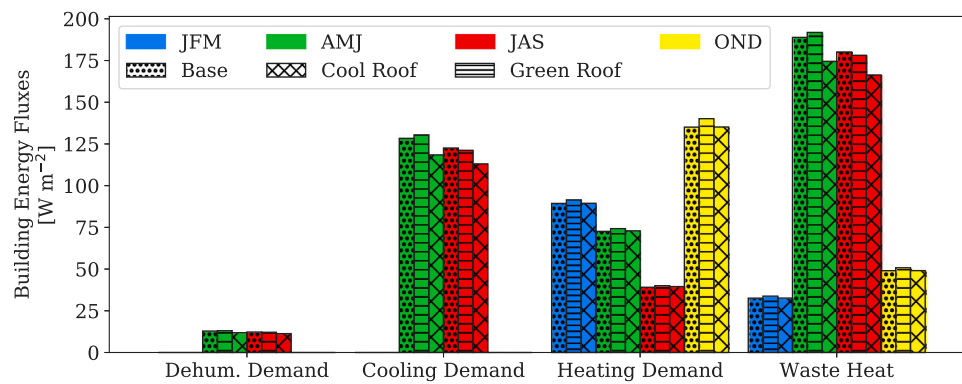
Fig. 12. Effects of green and cool roofs on building energy performance in different seasons; the building energy fluxes are mean of daily maximum over January–February–March (JFM), April–May–June (AMJ), July–August–September (JAS), and October–November–December (OND) in Vancouver 2007. (For interpretation of the references to color in this figure legend, the reader is referred to the web version of this article.)
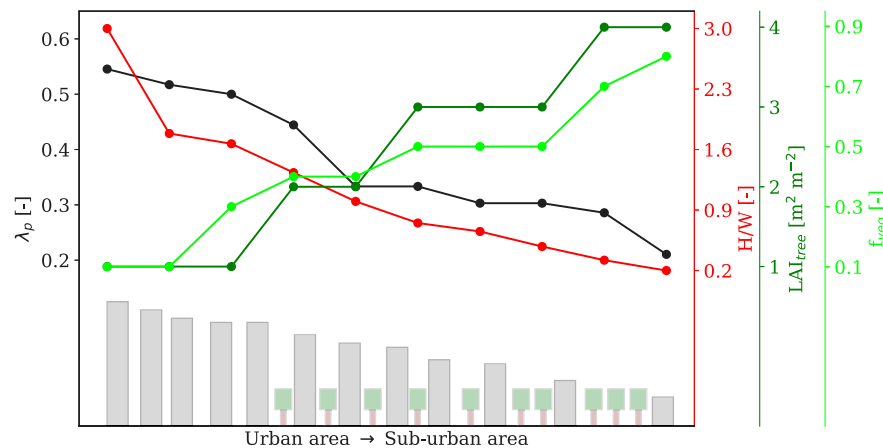

Fig. 13. Spatial variation of urban morphometric parameters including plan are density (λ_p [–]), leaf area index of urban trees (LAI_{tree} [m² m⁻²]), canyon aspect ratio (H/W [–]), and fraction of ground covered by vegetation (f_{veg} [–]) for a typical city.
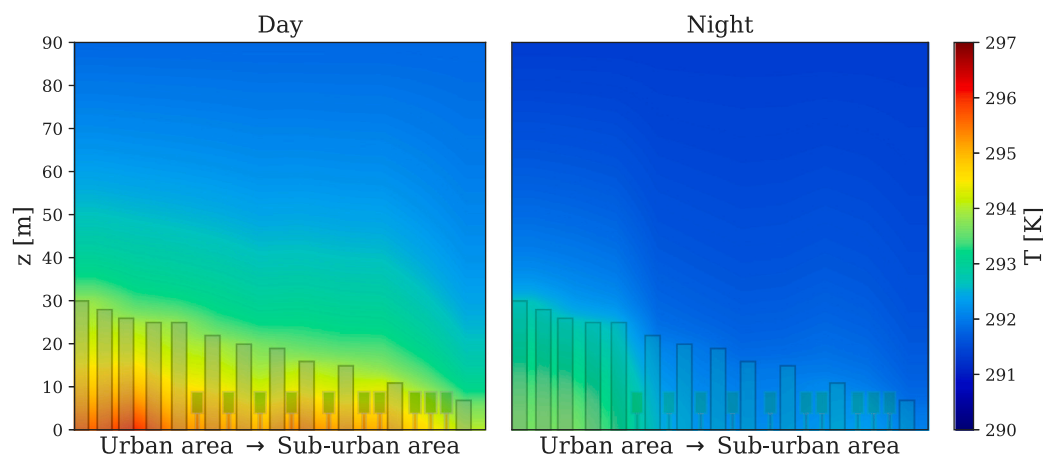
Fig. 14. Color plots of air potential temperature distribution from Local Climate Zone (LCZ) 1 to LCZ 9 at 1300 LST (left) and 2100 LST (right) in the summer; simulations are for Vancouver in July 2007. (For interpretation of the references to color in this figure legend, the reader is referred to the web version of this article.)

is consistent with expectations and comparable to the other urban climate models, simple parameterization of moisture source/sink terms and lack of forcing datasets near surface levels at rural sites restrict its application to non-rainy days and locations with available rural measurements. VCWG v2.0.0 is composed of the predecessor version's models (rural model, urban vertical diffusion model, building energy model, radiation model, and urban surface energy balance model) coupled with an urban hydrology model, and alternative options for

the forcing variables in the rural site and the option to instead provide meteorological boundary conditions at the top of the urban domain using meso-scale data products (e.g. ERA5 reanalysis dataset). The urban hydrology model is dynamically linked to the surface energy balance model and predicts surface and subsurface water balances and ecophysiological behavior of urban trees and low vegetation at the ground and roof levels.
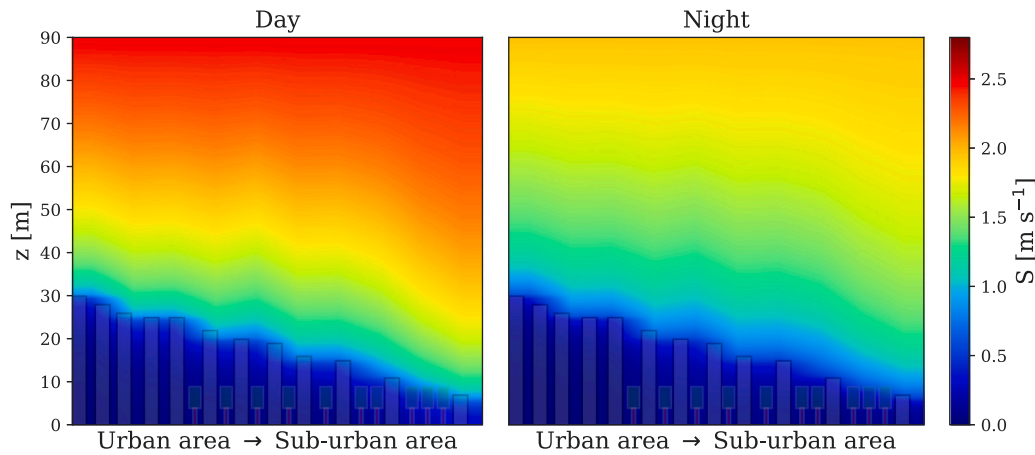
Fig. 15. Color plots of wind speed distribution from Local Climate Zone (LCZ) 1 to LCZ 9 at 1300 LST (left) and 2100 LST (right) in the summer; simulations are for Vancouver in July 2007. (For interpretation of the references to color in this figure legend, the reader is referred to the web version of this article.)
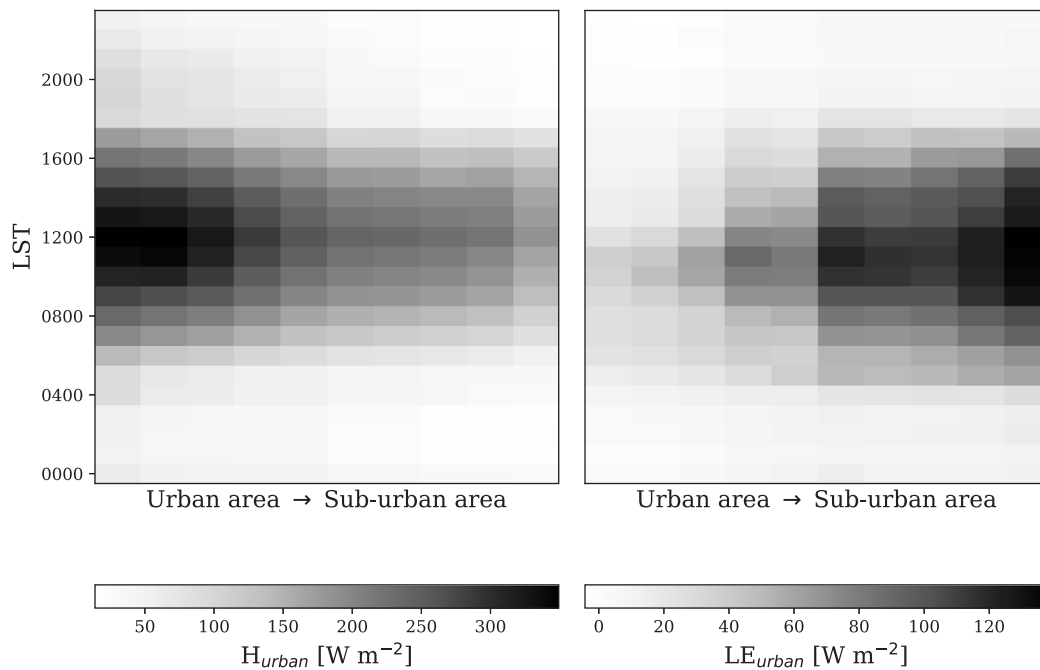

Fig. 16. Diurnal variation of sensible heat flux (left) and latent heat flux (right) of urban and sub-urban areas for LCZ 1 to LCZ 9.

The performance of VCWG v2.0.0 in predicting the potential temperature, wind speed, and specific humidity is evaluated against the BUBBLE dataset and the results from VCWG v1.3.2. The average RMSE of potential temperature, wind speed and specific humidity are improved by 0.5 [K], 0.52 [m s^{-1}], and 0.001 [kg kg^{-1}], respectively, and average R^2 [–] of potential temperature, wind speed and specific humidity are improved by 0.05, 0.04, and 0.56 [–], respectively. The capability of VCWG v2.0.0 to simulate urban sensible and latent heat fluxes is also evaluated against the BUBBLE and Vancouver Sunset datasets. The results show that VCWG v2.0.0 can predict the heat fluxes in reasonable agreement with the observed datasets. For the BUBBLE case, inclusion of urban hydrology reduces Bias and RMSE of sensible heat flux by 23.2 [W m^{-2}] and 29.2 [W m^{-2}], respectively, and increases the R^2 by 0.3 [–]. The statistics for latent heat flux also

exhibit an improvement, as absolute Bias and RMSE are decreased by 11.4 [W m^{-2}] and 14 [W m^{-2}], respectively, and R^2 is increased by 0.07 [–]. These statistics provide evidence that VCWG v2.0.0 represents an improvement relative to VCWG v1.3.2 because it provides more accurate predictions of urban climate variables. Various explorations of the model are also conducted, which include the study of model output variables in relation to seasonal variations, effects of ground vegetation, effects of green and cool roofs, and different Local Climate Zones (LCZ), in order to assess the performance of VCWG v2.0.0. The results obtained from these evaluations and explorations show that VCWG v2.0.0 can successfully overcome the limitations of VCWG v1.3.2 and combine most of the necessary models that are required for accurate prediction of urban climate variables.

While this study contributes to the development of a new urban climate model that overcomes several limitations of the previous studies,

other shortcomings remain. Further development is required to provide more realistic representation of a neighborhood and extend the single thermal zone building energy model to a multi zone model as well as development of a multilayer radiation model. VCWG can also be used as a diagnostic tool to investigate the simulation results obtained from complex models. Other models (e.g. an air pollution model) can be integrated into VCWG. The building energy model of VCWG can be adjusted to consider renewable energy technologies (e.g. solar collectors and wind turbines), which could result in more realistic estimation of building energy performance while using these technologies. VCWG can be improved to include snow processes. Also, VCWG can be investigated and improved in terms of its prediction of urban climate variables during extreme meteorological events (e.g. storms and flooding). At present, the VCWG model can account for the spatial variation of urban micro-climate variables in a computationally-efficient manner independent of an auxiliary meso-scale model. However, there is still a lack of representation of meteorological processes (such as advection, clouds, fogs, atmospheric meandering, etc.) that can only be captured by meso-scale models.

CRediT authorship contribution statement

Mohsen Moradi: Software, Data curation, Formal analysis, Investigation, Methodology, Validation, Visualization, Writing – original draft. **E. Scott Krayenhoff:** Conceptualization, Data curation, Investigation, Methodology, Supervision, Writing – review & editing. **Amir A. Aliabadi:** Conceptualization, Data curation, Formal analysis, Funding acquisition, Investigation, Methodology, Supervision, Writing – review & editing.

Declaration of competing interest

The authors declare that they have no known competing financial interests or personal relationships that could have appeared to influence the work reported in this paper.

Availability of code and data

The Atmospheric Innovations Research (AIR) Laboratory at the University of Guelph may provide the confidential supporting field data via the authorization of the data owners. The AIR lab will provide the model source code upon request. For access, contact Principal Investigator Amir A. Aliabadi (aliabadi@uoguelph.ca), contact the lead author Mohsen Moradi (moradim@uoguelph.ca), or visit http://www.aaa-scientists.com/.

Acknowledgments

Appendix

Radiation model

The incoming shortwave (both direct and diffuse) and longwave radiation fluxes from the sky are retrieved from an EPW file or the ERA5 dataset. The net allwave radiation flux on a surface is the sum of the net shortwave and longwave radiation fluxes

$$R_n = S^\downarrow - S^\uparrow + L^\downarrow - L^\uparrow, \tag{11}$$

where $S^\downarrow$, $S^\uparrow$, $L^\downarrow$, and $L^\uparrow$ [W m^{-2}] are the incident shortwave, leaving shortwave, incident longwave, and leaving longwave radiation fluxes. The absorbed (net) shortwave radiation on surface element i is given by

$$S_{n,i} = (1 - \alpha_i)\left(S_i^\downarrow\right) = (1 - \alpha_i)\left(S_i^{\downarrow\text{direct}} + S_i^{\downarrow\text{diffuse}}\right), \tag{12}$$

where α_i [–] is the albedo of the surface and $S_i^{\downarrow\text{direct}}$ and $S_i^{\downarrow\text{diffuse}}$ [W m^{-2}] are the direct and diffuse incident shortwave radiation fluxes to surface element i. In our notation i can be R, G, W, or V for roof, ground, wall, and vegetation, respectively.

The absorbed (net) longwave radiation for each surface element is calculated by

$$L_{n,i} = \varepsilon_i \left(L_i^\downarrow - \sigma T_i^4\right), \tag{13}$$

where ε_i [–] is the emissivity of the urban surface element, $L_i^\downarrow$ [W m^{-2}] is the incident longwave radiation flux, $\sigma = 5.67 \times 10^{-8}$ W m^{-2} K^{-4} is the Stefan Boltzmann constant, and T_i [K] is the surface element temperature.

Surface energy balance model

Sensible heat flux

The resistances for the horizontal surfaces covered by vegetation r_{veg}, bare soil r_{bare}, and impervious r_{imp} [s m^{-1}] can be formulated as [50,101]

$$r_{\text{imp}} = r_{\text{aero}}, \tag{14}$$

$$r_{\text{bare}} = r_{\text{aero}}, \tag{15}$$

$$r_{\text{veg}} = r_{\text{aero}} + \hat{r}_{\text{lb,veg}}, \tag{16}$$

where r_{aero} [s m^{-1}] is aerodynamic resistance and $\hat{r}_{\text{lb,veg}}$ [s m^{-1}] is the re-scaled leaf boundary resistance. The aerodynamic resistance is based on the study by Louis [57] and can be calculated as [57]

$$r_{\text{aero}} = R_{\text{drag}} \frac{\left(\ln \frac{z}{z_0}\right)^2}{\overline{S}_z \kappa^2} \frac{1}{F_h\left(\frac{z}{z_0}, Ri_B\right)}, \tag{17}$$

where $R_{\text{drag}} = 0.74$ [–] is ratio of the drag coefficients for momentum to heat [53], Ri_B [–] is the bulk Richardson number, $\kappa = 0.4$ is von Kármán constant, z_0 [m] is aerodynamic roughness length of the surface, and $\overline{S}_z$ [m s^{-1}] is wind speed near the surface, and F_h [–] is the stability function for sensible heat flux.

Re-scaling $r_{\text{lb,veg}}$ [s m^{-1}] by a factor of 2, the leaf area index LAI_{veg} [m^2 m^{-2}], and the stem area index SAI_{veg} [m^2 m^{-2}] account for two-sided resistance of the leaf and the whole vegetation canopy [50,101]

$$\hat{r}_{\text{lb,veg}} = \frac{r_{\text{lb,veg}}}{2(LAI_{\text{veg}} + SAI_{\text{veg}})}. \tag{18}$$

Detailed calculation of leaf boundary resistance is provided in Moradi [74].

The sunlit and shaded walls are assumed to be impervious and the thermal resistance between the surface and adjacent atmosphere can be formulated as [102]

$$r_{\text{wall}} = \frac{1}{h_{\text{c}}}, \tag{19}$$

where $h_{\text{c}} = 5.678(1.09 + 0.23(\overline{S}_{\text{z}}/0.3048))$ [m s^{-1}] is an empirical convective heat transfer coefficient calculated as a function of the vertical profile of wind speed in the canyon.

The thermal resistance for tree r_{tree} [s m^{-1}] can be calculated using Eq. (16). The leaf boundary resistance of trees ($r_{\text{lb,tree}}$ [s m^{-1}]) can be calculated using the formulation provided in Moradi [74], with adopted parameters for trees. The undercanopy resistance approach is used to calculate the aerodynamic resistance (r_{aero} [s m^{-1}]) from the tree to the canyon [103].

Latent heat flux

The evaporative fluxes at the ground and roof levels are caused by evaporation from runon at the impervious ground E_{imp}, evaporation from runon at the bare ground E_{bare}, evaporation from runon at the soil surface underneath the low vegetation E_{veg}, evaporation from intercepted water on low vegetation $E_{\text{veg,int}}$, transpiration from sunlit low vegetation $TE_{\text{veg,sun}}$, and transpiration from shaded low vegetation $TE_{\text{veg,shd}}$, and they are all in [kg m^{-2} s^{-1}]. The resistance for the horizontal surfaces used in the calculation of latent heat fluxes are [50]

$$r_{\text{imp}} = r_{\text{aero}} \tag{20}$$

$$r_{\text{bare}} = r_{\text{aero}} + r_{\text{soil}} \tag{21}$$

$$r_{\text{veg}} = r_{\text{aero}} + r_{\text{soil}} \tag{22}$$

$$r_{\text{veg,int}} = r_{\text{aero}} + \hat{r}_{\text{lb,veg}} \tag{23}$$

$$r_{\text{veg,sun}} = r_{\text{aero}} + \hat{r}_{\text{lb,veg,sun}} + \hat{r}_{\text{s,veg,sun}} \tag{24}$$

$$r_{\text{veg,shd}} = r_{\text{aero}} + \hat{r}_{\text{lb,veg,shd}} + \hat{r}_{\text{s,veg,shd}} \tag{25}$$

where r_{aero} [s m^{-1}] is aerodynamic resistance which can be calculated from Eq. (17), r_{soil} is the soil resistance, $\hat{r}_{\text{lb,veg}}$ is the re-scaled leaf boundary resistance of low vegetation, and $\hat{r}_{\text{s,veg}}$ is the re-scaled stomatal resistance all in [s m^{-1}]. The subscript sun and shd denote the sunlit and shaded part of the vegetation, respectively. The re-scaled stomatal resistance can be calculated as [50,101]

$$\hat{r}_{\text{lb,veg}} = \frac{r_{\text{lb,veg}}}{(LAI_{\text{veg}} + SAI_{\text{veg}})d_{\text{w,veg}}} \tag{26}$$

$$\hat{r}_{\text{lb,veg,sun}} = \frac{r_{\text{lb,veg}}}{LAI_{\text{veg}} F_{\text{sun,veg}}(1 - d_{\text{w,veg}})} \tag{27}$$

$$\hat{r}_{\text{lb,veg,shd}} = \frac{r_{\text{lb,veg}}}{LAI_{\text{veg}} F_{\text{shd,veg}}(1 - d_{\text{w,veg}})} \tag{28}$$

$$\hat{r}_{\text{s,veg,sun}} = \frac{r_{\text{s,veg,sun}}}{LAI_{\text{veg}} F_{\text{sun,veg}}(1 - d_{\text{w,veg}})} \tag{29}$$

$$\hat{r}_{\text{s,veg,shd}} = \frac{r_{\text{s,veg,shd}}}{LAI_{\text{veg}} F_{\text{shd,veg}}(1 - d_{\text{w,veg}})}, \tag{30}$$

where $r_{\text{lb,veg}}$ [s m^{-1}] is leaf boundary resistance, $r_{\text{s,veg,sun}}$ and $r_{\text{s,veg,shd}}$ are stomatal resistance of the sunlit and shaded part of the vegetation all in [s m^{-1}], $d_{\text{w,veg}}$ [–] is the fraction of vegetation covered by intercepted water, and $F_{\text{sun,veg}}$ and $F_{\text{shd,veg}}$ [–] are fraction of sunlit and shaded vegetation, respectively. The detailed calculation of soil, leaf boundary, and stomatal resistances are provided in Moradi [74]. The shaded and sunlit fractions of low vegetation are calculated based on the assumption of exponential decay of direct radiation within the vegetation canopy as [50]

$$F_{\text{sun,veg}} = \frac{1}{LAI_{\text{veg}}} \frac{1 - e^{(-K_{\text{opt}} LAI_{\text{veg}})}}{K_{\text{opt}}}, \tag{31}$$

$$F_{\text{shd,veg}} = 1 - F_{\text{sun,veg}}, \tag{32}$$

where $K_{\text{opt}} = 0.5$ [–] is light transmission coefficient. Eqs. (20)–(22) are the resistances used to calculate evaporation from surfaces and Eqs. (24) and (25) are the resistances used to calculate transpiration from vegetation. As detailed in Eqs. (26)–(30), the fraction of canopy covered by intercepted water $d_{\text{w,veg}}$ [–] contributes to evaporation from intercepted water, while the rest of it contributes to transpiration $(1 - d_{\text{w,veg}})$ [–], and $d_{\text{w,veg}}$ [–] can be calculated as [50]

$$d_{\text{w,veg}} = \min\left[1, (Int/Int_{\max})^{2/3}\right], \tag{33}$$

where Int [mm] is the intercepted water and $Int_{\max}$ [mm] is maximum interception capacity of the surface.

The latent heat flux from tree accounts for evaporation from intercepted water and transpiration from sunlit and shaded fractions of the tree. The thermal resistances can be formulated as follows [50]

$$r_{\text{tree,int}} = r_{\text{tree}} + \hat{r}_{\text{lb,tree}}, \tag{34}$$

$$r_{\text{tree,sun}} = r_{\text{tree}} + \hat{r}_{\text{lb,tree,sun}} + r_{\text{s,tree,sun}}, \tag{35}$$

$$r_{\text{tree,shd}} = r_{\text{tree}} + \hat{r}_{\text{lb,tree,shd}} + r_{\text{s,tree,shd}}, \tag{36}$$

where $r_{\text{tree,int}}$, $r_{\text{tree,sun}}$, and $r_{\text{tree,shd}}$ all in [s m^{-1}] are used to determine latent heat flux of intercepted water on trees LE_{tree} [W m^{-2}], latent heat of transpiration from sunlit faction $LTE_{\text{tree,sun}}$ [W m^{-2}], and latent heat of transpiration from shaded fraction $LTE_{\text{tree,shd}}$ [W m^{-2}], respectively. $\hat{r}_{\text{lb,tree}}$ [s m^{-1}] is the re-scaled leaf boundary resistance of tree, $\hat{r}_{\text{lb,tree,sun}}$ and $\hat{r}_{\text{lb,tree,shd}}$ [s m^{-1}] are re-scaled leaf boundary resistance of sunlit and shaded fractions of the tree respectively, and $\hat{r}_{\text{s,tree,sun}}$ and $\hat{r}_{\text{s,tree,shd}}$ [s m^{-1}] are the re-scaled soil resistances for the sunlit and shaded fractions of the canopy, respectively. The resistances can be calculated as [50]

$$\hat{r}_{\text{lb,tree}} = \frac{r_{\text{lb,tree}}}{(LAI_{\text{tree}} + SAI_{\text{t}})d_{\text{w,tree}}} \tag{37}$$

$$\hat{r}_{\text{lb,tree,sun}} = \frac{r_{\text{lb,tree}}}{LAI_{\text{tree}} F_{\text{sun,tree}}(1 - d_{\text{w,tree}})} \tag{38}$$

$$\hat{r}_{\text{lb,tree,shd}} = \frac{r_{\text{lb,tree}}}{LAI_{\text{tree}} F_{\text{shd,tree}}(1 - d_{\text{w,tree}})} \tag{39}$$

$$\hat{r}_{\text{s,tree,sun}} = \frac{r_{\text{s,tree,sun}}}{LAI_{\text{tree}} F_{\text{sun,tree}}(1 - d_{\text{w,tree}})} \tag{40}$$

$$\hat{r}_{\text{s,tree,shd}} = \frac{r_{\text{s,tree,shd}}}{LAI_{\text{tree}} F_{\text{shd,tree}}(1 - d_{\text{w,tree}})}, \tag{41}$$

where $r_{\text{lb,tree}}$ is leaf boundary resistance, $r_{\text{s,sun}}$ and $r_{\text{s,shd}}$ are stomatal resistances of the sunlit and shaded part of the tree, respectively, all in [s m^{-1}], $d_{\text{w,tree}}$ [–] is the fraction of tree covered by intercepted water, and $F_{\text{sun,tree}}$ and $F_{\text{shd,tree}}$ [–] are fractions of sunlit and shaded tree, respectively. The detailed calculation of soil, leaf boundary, and stomatal resistances are provided in Moradi [74].

Urban vertical diffusion model

The momentum equations can be written as [70]

$$\frac{\partial \overline{U}}{\partial t} = -\underbrace{\frac{\partial \overline{uw}}{\partial z}}_{\text{I}} - \underbrace{\frac{1}{\rho} \frac{\partial \overline{P}}{\partial x}}_{\text{II}} - \underbrace{D_{\text{x}}}_{\text{III}}, \tag{42}$$

$$\frac{\partial \overline{V}}{\partial t} = -\underbrace{\frac{\partial \overline{vw}}{\partial z}}_{\text{I}} - \underbrace{\frac{1}{\rho} \frac{\partial \overline{P}}{\partial y}}_{\text{II}} - \underbrace{D_{\text{y}}}_{\text{III}}, \tag{43}$$

where $\overline{U}$ and $\overline{V}$ [m s^{-1}] are cross- and along-canyon wind velocity vector components, term I is the vertical gradient of momentum flux, term II is acceleration caused by pressure gradient, and term III is drag caused by buildings and trees. Parameterization of these terms are based on CFD simulations by Martilli and Santiago [104], Santiago and Martilli [70], Krayenhoff et al. [20], and Nazarian et al. [105]. The vertical gradient of fluxes are parameterized using the K-theory, in which the $k - \ell$ turbulence model is used to calculate the turbulent

diffusion coefficient. The equation for turbulence kinetic energy k can be written as [70]

$$\frac{\partial k}{\partial t} = \underbrace{K_{\mathrm{m}} \left[\left(\frac{\partial \overline{U}}{\partial z} \right)^2 + \left(\frac{\partial \overline{V}}{\partial z} \right)^2 \right]}_{\text{I}} + \underbrace{\frac{\partial}{\partial z} \left(\frac{K_{\mathrm{m}}}{\sigma_{\mathrm{k}}} \frac{\partial k}{\partial z} \right)}_{\text{II}} - \underbrace{\frac{g}{\Theta_0} \frac{K_{\mathrm{m}}}{Pr_{\mathrm{t}}} \frac{\partial \overline{\Theta}}{\partial z}}_{\text{III}}$$
$$+ \underbrace{S_{\text{wake}}}_{\text{IV}} - \underbrace{\varepsilon}_{\text{V}}, \tag{44}$$

where term I is shear production, term II is the turbulent transport of kinetic energy, term III is buoyant production/dissipation, term IV is wake production by buildings and trees, and term V is dissipation. The transport equations for the potential temperature and specific humidity can be written as [70]

$$\frac{\partial \overline{\Theta}}{\partial t} = \underbrace{\frac{\partial}{\partial z} \left(\frac{K_{\mathrm{m}}}{Pr_{\mathrm{t}}} \frac{\partial \overline{\Theta}}{\partial z} \right)}_{\text{I}} + \underbrace{S_{\Theta}}_{\text{II}}, \tag{45}$$

$$\frac{\partial \overline{Q}}{\partial t} = \underbrace{\frac{\partial}{\partial z} \left(\frac{K_{\mathrm{m}}}{Sc_{\mathrm{t}}} \frac{\partial \overline{Q}}{\partial z} \right)}_{\text{I}} + \underbrace{S_{\mathrm{Q}}}_{\text{II}}, \tag{46}$$

where $\overline{\Theta}$ [K] is the air potential temperature, $\overline{Q}$ [kg kg^{-1}] is the air specific humidity, term I represents the turbulent transport of potential temperature/specific humidity, and term II accounts for the sink/source terms corresponding to sensible/latent heat and evaporative fluxes, which are obtained from the surface energy and water balance models. More details about the calculation of sink and source terms in the transport equations are provided in studies by Krayenhoff et al. [20] and Moradi et al. [51].

References

[1] T.R. Oke, G. Mills, A. Christen, J.A. Voogt, Urban Climates, Cambridge University Press, Cambridge, 2017, http://dx.doi.org/10.1017/9781139016476.

[2] T.R. Oke, G.T. Johnson, D.G. Steyn, I.D. Watson, Simulation of surface urban heat islands under 'ideal' conditions at night Part 2: Diagnosis of causation, Bound.-Lay. Meteorol. 56 (4) (1991) 339–358, http://dx.doi.org/10.1007/BF00119211.

[3] C.S.B. Grimmond, M. Best, J. Barlow, A.J. Arnfield, J.-J. Baik, A. Baklanov, S. Belcher, M. Bruse, I. Calmet, F. Chen, P. Clark, A. Dandou, E. Erell, K. Fortuniak, R. Hamdi, M. Kanda, T. Kawai, H. Kondo, S. Krayenhoff, S.H. Lee, S.-B. Limor, A. Martilli, V. Masson, S. Miao, G. Mills, R. Moriwaki, K. Oleson, A. Porson, U. Sievers, M. Tombrou, J. Voogt, T. Williamson, Urban surface energy balance models: model characteristics and methodology for a comparison study, in: A. Baklanov, C.S.B. Grimmond, A. Mahura, A.M. Athanassiadou (Eds.), Meteorological and Air Quality Models for Urban Areas, Springer, 2009, http://dx.doi.org/10.1007/978-3-642-00298-4.

[4] M.G. Mansell, Rural and Urban Hydrology, Thomas Telford, London, 2003, http://dx.doi.org/10.1680/rauh.32309.0007.

[5] C.S.B. Grimmond, T.R. Oke, Aerodynamic properties of urban areas derived from analysis of surface form, J. Appl. Meteorol. 38 (9) (1999) 1262–1292, http://dx.doi.org/10.1175/1520-0450(1999)038<1262:APOUAD>2.0.CO;2.

[6] S. Dupont, T.L. Otte, J.K.S. Ching, Simulation of meteorological fields within and above urban and rural canopies with a mesoscale model, Bound.-Lay. Meteorol. 113 (1) (2004) 111–158, http://dx.doi.org/10.1023/B:BOUN.0000037327.19159.ac.

[7] S. Saneinejad, P. Moonen, T. Defraeye, D. Derome, J. Carmeliet, Coupled CFD, radiation and porous media transport model for evaluating evaporative cooling in an urban environment, J. Wind Eng. Ind. Aerodyn. 104–106 (2012) 455–463, http://dx.doi.org/10.1016/j.jweia.2012.02.006.

[8] B. Blocken, Computational fluid dynamics for urban physics: Importance, scales, possibilities, limitations and ten tips and tricks towards accurate and reliable simulations, Build. Environ. 91 (2015) 219–245, http://dx.doi.org/10.1016/j.buildenv.2015.02.015.

[9] N. Nazarian, J. Kleissl, Realistic solar heating in urban areas: air exchange and street-canyon ventilation, Build. Environ. 95 (2016) 75–93, http://dx.doi.org/10.1016/j.buildenv.2015.08.021.

[10] A.A. Aliabadi, E.S. Krayenhoff, N. Nazarian, L.W. Chew, P.R. Armstrong, A. Afshari, L.K. Norford, Effects of roof-edge roughness on air temperature and pollutant concentration in urban canyons, Bound.-Lay. Meteorol. 164 (2) (2017) 249–279, http://dx.doi.org/10.1007/s10546-017-0246-1.

[11] A.A. Aliabadi, N. Veriotes, G. Pedro, A Very Large-Eddy Simulation (VLES) model for the investigation of the neutral atmospheric boundary layer, J. Wind Eng. Ind. Aerodyn. 183 (2018) 152–171, http://dx.doi.org/10.1016/j.jweia.2018.10.014.

[12] N. Nazarian, A. Martilli, J. Kleissl, Impacts of realistic urban heating, Part I: spatial variability of mean flow, turbulent exchange and pollutant dispersion, Bound.-Lay. Meteorol. 166 (3) (2018) 367–393, http://dx.doi.org/10.1007/s10546-017-0311-9.

[13] M. Ahmadi-Baloutaki, A.A. Aliabadi, A very large-eddy simulation model using a reductionist inlet turbulence generator and wall modeling for stable atmospheric boundary layers, Fluid Dyn. 56 (3) (2021) 413–432, http://dx.doi.org/10.1134/S0015462821020026.

[14] V. Masson, A physically-based scheme for the urban energy budget in atmospheric models, Bound.-Lay. Meteorol. 94 (3) (2000) 357–397, http://dx.doi.org/10.1023/A:1002463829265.

[15] H. Kusaka, H. Kondo, Y. Kikegawa, F. Kimura, A simple single-layer urban canopy model for atmospheric models: comparison with multi-layer and slab models, Bound.-Lay. Meteorol. 101 (3) (2001) 329–358, http://dx.doi.org/10.1023/A:1019207923078.

[16] H.-N.S. Chin, M.J. Leach, G.A. Sugiyama, J.M. Leone Jr., H. Walker, J.S. Nasstrom, M.J. Brown, Evaluation of an urban canopy parameterization in a mesoscale model using VTMX and URBAN 2000 Data, Mon. Weather Rev. 133 (7) (2005) 2043–2068, http://dx.doi.org/10.1175/MWR2962.1.

[17] A. Martilli, A. Clappier, M.W. Rotach, An urban surface exchange parameterisation for mesoscale models, Bound.-Lay. Meteorol. 104 (2) (2002) 261–304, http://dx.doi.org/10.1023/A:1016099921195.

[18] O. Coceal, S.E. Belcher, A canopy model of mean winds through urban areas, Q. J. R. Meteorol. Soc. 130 (599) (2004) 1349–1372, http://dx.doi.org/10.1256/qj.03.40.

[19] E.S. Krayenhoff, A. Christen, A. Martilli, T.R. Oke, A multi-layer radiation model for urban neighbourhoods with trees, Bound.-Lay. Meteorol. 151 (1) (2014) 139–178, http://dx.doi.org/10.1007/s10546-013-9883-1.

[20] E.S. Krayenhoff, J.-L. Santiago, A. Martilli, A. Christen, T.R. Oke, Parametrization of drag and turbulence for urban neighbourhoods with trees, Bound.-Lay. Meteorol. 156 (2) (2015) 157–189, http://dx.doi.org/10.1007/s10546-015-0028-6.

[21] A.A. Aliabadi, M. Moradi, D. Clement, W.D. Lubitz, B. Gharabaghi, Flow and temperature dynamics in an urban canyon under a comprehensive set of wind directions, wind speeds, and thermal stability conditions, Environ. Fluid Mech. 19 (1) (2019) 81–109, http://dx.doi.org/10.1007/s10652-018-9606-8.

[22] B. Bueno, L.K. Norford, J. Hidalgo, G. Pigeon, The urban weather generator, J. Build. Perform. Simul. 6 (4) (2012) 269–281, http://dx.doi.org/10.1080/19401493.2012.718797.

[23] E. Erell, T. Williamson, Simulating air temperature in an urban street canyon in all weather conditions using measured data at a reference meteorological station, Int. J. Climatol. 26 (12) (2006) 1671–1694, http://dx.doi.org/10.1002/joc.1328.

[24] G. Mills, An urban canopy-layer climate model, Theor. Appl. Climatol. 57 (3–4) (1997) 229–244, http://dx.doi.org/10.1007/BF00863615.

[25] F. Salamanca, A. Krpo, A. Martilli, A. Clappier, A new building energy model coupled with an urban canopy parameterization for urban climate simulations-part I. formulation, verification, and sensitivity analysis of the model, Theor. Appl. Climatol. 99 (3–4) (2010) 331–344, http://dx.doi.org/10.1007/s00704-009-0142-9.

[26] Y.-H. Ryu, J.-J. Baik, S.-H. Lee, A new single-layer urban canopy model for use in mesoscale atmospheric models, J. Appl. Meteorol. Climatol. 50 (9) (2011) 1773–1794, http://dx.doi.org/10.1175/2011JAMC2665.1.

[27] B. Bueno, M. Roth, L.K. Norford, R. Li, Computationally efficient prediction of canopy level urban air temperature at the neighbourhood scale, Urban Clim. 9 (2014) 35–53, http://dx.doi.org/10.1016/j.uclim.2014.05.005.

[28] V. Masson, C.S.B. Grimmond, T.R. Oke, Evaluation of the Town Energy Balance (TEB) scheme with direct measurements from dry districts in two cities, J. Appl. Meteorol. Climatol. 41 (10) (2002) 1011–1026, http://dx.doi.org/10.1175/1520-0450(2002)041<1011:EOTTEB>2.0.CO;2.

[29] E.S. Krayenhoff, J.A. Voogt, A microscale three-dimensional urban energy balance model for studying surface temperatures, Bound.-Lay. Meteorol. 123 (3) (2007) 433–461, http://dx.doi.org/10.1007/s10546-006-9153-6.

[30] E.S. Krayenhoff, T. Jiang, A. Christen, A. Martilli, T.R. Oke, B.N. Bailey, N. Nazarian, J.A. Voogt, M.G. Giometto, A. Stastny, et al., A multi-layer urban canopy meteorological model with trees (BEP-Tree): Street tree impacts on pedestrian-level climate, Urban Clim. 32 (2020) 100590, http://dx.doi.org/10.1016/j.uclim.2020.100590.

[31] M. Roth, Review of atmospheric turbulence over cities, Q. J. R. Meteorol. Soc. 126 (564) (2000) 941–990, http://dx.doi.org/10.1002/qj.49712656409.

[32] V. Masson, L. Gomes, G. Pigeon, C. Liousse, V. Pont, J.P. Lagouarde, J. Voogt, J. Salmond, T.R. Oke, J. Hidalgo, D. Legain, O. Garrouste, C. Lac, O. Connan, X. Briottet, S. Lachérade, P. Tulet, The Canopy and Aerosol Particles Interactions in TOlouse Urban Layer (CAPITOUL) experiment, Meteorol. Atmos. Phys. 102 (2008) 135–157, http://dx.doi.org/10.1007/s00703-008-0289-4.

[33] D. Zajic, H.J.S. Fernando, R. Calhoun, M. Princevac, M.J. Brown, E.R. Pardyjak, Flow and turbulence in an urban canyon, J. Appl. Meteorol. Climatol. 50 (1) (2011) 203–223, http://dx.doi.org/10.1175/2010JAMC2525.1.

[34] Y. Kikegawa, Y. Genchi, H. Yoshikado, H. Kondo, Development of a numerical simulation system toward comprehensive assessments of urban warming countermeasures including their impacts upon the urban buildings' energy-demands, Appl. Energy 76 (4) (2003) 449–466, http://dx.doi.org/10.1016/S0306-2619(03)00009-6.

[35] N. Yaghoobian, J. Kleissl, Effect of reflective pavements on building energy use, Urban Clim. 2 (2012) 25–42, http://dx.doi.org/10.1016/j.uclim.2012.09.002.

[36] F. Chen, H. Kusaka, R. Bornstein, J. Ching, C.S.B. Grimmond, S. Grossman-Clarke, T. Loridan, K.W. Manning, A. Martilli, S. Miao, D. Sailor, F.P. Salamanca, H. Taha, M. Tewari, X. Wang, A.A. Wyszogrodzki, C. Zhang, The integrated WRF/urban modelling system: development, evaluation, and applications to urban environmental problems, Int. J. Climatol. 31 (2) (2011) 273–288, http://dx.doi.org/10.1002/joc.2158.

[37] P. Conry, H. Fernando, L. Leo, A. Sharma, M. Potosnak, J. Hellmann, Multi-scale simulations of climate-change influence on chicago heat island, in: ASME 2014 4th Joint US-European Fluids Engineering Division Summer Meeting Collocated with the ASME 2014 12th International Conference on Nanochannels, Microchannels, and Minichannels, American Society of Mechanical Engineers, Chicago, Illinois, USA, 2014, http://dx.doi.org/10.1115/FEDSM2014-21581.

[38] A.K. Kochanski, E.R. Pardyjak, R. Stoll, A. Gowardhan, M.J. Brown, W.J. Steenburgh, One-way coupling of the WRF-QUIC urban dispersion modeling system, J. Appl. Meteorol. Climatol. 54 (10) (2015) 2119–2139, http://dx.doi.org/10.1175/JAMC-D-15-0020.1.

[39] D. Mauree, N. Blond, A. Clappier, Multi-scale modeling of the urban meteorology: Integration of a new canopy model in the WRF model, Urban Clim. 26 (2018) 60–75, http://dx.doi.org/10.1016/j.uclim.2018.08.002.

[40] F. Salamanca, M. Georgescu, A. Mahalov, M. Moustaoui, M. Wang, Anthropogenic heating of the urban environment due to air conditioning, J. Geophys. Res.: Atmos. 119 (10) (2014) 5949–5965, http://dx.doi.org/10.1002/2013JD021225.

[41] C.S.B. Grimmond, C. Souch, M.D. Hubble, Influence of tree cover on summertime surface energy balance fluxes, San Gabriel Valley, Los Angeles, Clim. Res. 6 (1) (1996) 45–57, http://dx.doi.org/10.3354/cr006045.

[42] H. Akbari, M. Pomerantz, H. Taha, Cool surfaces and shade trees to reduce energy use and improve air quality in urban areas, Sol. Energy 70 (3) (2001) 295–310, http://dx.doi.org/10.1016/S0038-092X(00)00089-X.

[43] J.R. Simpson, E.G. McPherson, Potential of tree shade for reducing residential energy use in California, J. Arboric. 22 (1) (1996) 10–18.

[44] H. Akbari, Shade trees reduce building energy use and CO_2 emissions from power plants, Environ. Pollut. 116 (2002) S119–S126, http://dx.doi.org/10.1016/S0269-7491(01)00264-0.

[45] C. Wang, Z.-H. Wang, J. Yang, Cooling effect of urban trees on the built environment of contiguous United States, Earth's Future 6 (8) (2018) 1066–1081, http://dx.doi.org/10.1029/2018EF000891.

[46] L. Järvi, C.S.B. Grimmond, A. Christen, The Surface Urban Energy and Water balance Scheme (SUEWS): Evaluation in Los Angeles and Vancouver, J. Hydrol. 411 (3–4) (2011) 219–237, http://dx.doi.org/10.1016/j.jhydrol.2011.10.001.

[47] S.Z. Husain, N. Alavi, S. Bélair, M. Carrera, S. Zhang, V. Fortin, M. Abrahamowicz, N. Gauthier, The multibudget Soil, Vegetation, and Snow (SVS) scheme for land surface parameterization: Offline warm season evaluation, J. Hydrometeorol. 17 (8) (2016) 2293–2313, http://dx.doi.org/10.1175/JHM-D-15-0228.1.

[48] Z.-H. Wang, E. Bou-Zeid, J.A. Smith, A coupled energy transport and hydrological model for urban canopies evaluated using a wireless sensor network, Q. J. Meteorol. Soc. 139 (675) (2013) 1643–1657, http://dx.doi.org/10.1002/qj.2032.

[49] J. Yang, Z.-H. Wang, M. Georgescu, F. Chen, M. Tewari, Assessing the impact of enhanced hydrological processes on urban hydrometeorology with application to two cities in contrasting climates, J. Hydrometeorol. 17 (4) (2016) 1031–1047, http://dx.doi.org/10.1175/JHM-D-15-0112.1.

[50] N. Meili, G. Manoli, P. Burlando, E. Bou-Zeid, W.T.L. Chow, A.M. Coutts, E. Daly, K.A. Nice, M. Roth, N.J. Tapper, E. Velasco, E.R. Vivoni, S. Fatichi, An urban ecohydrological model to quantify the effect of vegetation on urban climate and hydrology (UT&C v1.0), Geosci. Model Dev. 13 (1) (2020) 335–362, http://dx.doi.org/10.5194/gmd-13-335-2020.

[51] M. Moradi, B. Dyer, A. Nazem, M.K. Nambiar, M.R. Nahian, B. Bueno, C. Mackey, S. Vasanthakumar, N. Nazarian, E.S. Krayenhoff, L.K. Norford, A.A. Aliabadi, The Vertical City Weather Generator (VCWG v1.3.2), Geosci. Model Dev. 14 (2) (2021) 961–984, http://dx.doi.org/10.5194/gmd-14-961-2021.

[52] A.S. Monin, A.M. Obukhov, Basic regularity in turbulent mixing in the surface layer of the atmosphere, Tr. Akad. Nauk SSSR Geophiz. Inst. (24) (1957) 163–187.

[53] J.A. Businger, J.C. Wyngaard, Y. Izumi, E.F. Bradley, Flux-profile relationships in the atmospheric surface layer, J. Atmos. Sci. 28 (2) (1971) 181–189, http://dx.doi.org/10.1175/1520-0469(1971)028<0181:FPRITA>2.0.CO;2.

[54] A.J. Dyer, A review of flux-profile relationships, Bound.-Lay. Meteorol. 7 (3) (1974) 363–372, http://dx.doi.org/10.1007/BF00240838.

[55] H.L. Penman, Natural evaporation from open water, bare soil and grass, Proc. R. Soc. Lond. Ser. A Math. Phys. Sci. 193 (1032) (1948) 120–145.

[56] J.L. Monteith, Evaporation and environment, in: Symposia of the Society for Experimental Biology, Vol. 19, Cambridge University Press, Cambridge, 1965, pp. 205–234.

[57] J.-F. Louis, A parametric model of vertical eddy fluxes in the atmosphere, Bound.-Lay. Meteorol. 17 (2) (1979) 187–202, http://dx.doi.org/10.1007/BF00117978.

[58] R.G. Allen, M. Smith, L.S. Pereira, A. Perrier, An update for the calculation of reference evapotranspiration, ICID Bull. 43 (2) (1994) 35–92.

[59] Y.-H. Ryu, E. Bou-Zeid, Z.-H. Wang, J.A. Smith, Realistic representation of trees in an urban canopy model, Bound.-Lay. Meteorol. 159 (2016) 193–220, http://dx.doi.org/10.1007/s10546-015-0120-y.

[60] Z.-H. Wang, Geometric effect of radiative heat exchange in concave structure with application to heating of steel I-sections in fire, Int. J. Heat Mass Transfer 53 (5–6) (2010) 997–1003, http://dx.doi.org/10.1016/j.ijheatmasstransfer.2009.11.013.

[61] Z.-H. Wang, Monte Carlo simulations of radiative heat exchange in a street canyon with trees, Sol. Energy 110 (2014) 704–713, http://dx.doi.org/10.1016/j.solener.2014.10.012.

[62] S.-H. Lee, S.-U. Park, A vegetated urban canopy model for meteorological and environmental modelling, Bound.-Lay. Meteorol. 126 (1) (2008) 73–102, http://dx.doi.org/10.1007/s10546-007-9221-6.

[63] A. Frank, W. Heidemann, K. Spindler, Modeling of the surface-to-surface radiation exchange using a Monte Carlo method, J. Phys. Conf. Ser. 745 (3) (2016) 032143, http://dx.doi.org/10.1088/1742-6596/745/3/032143.

[64] I. Rodriguez-Iturbe, A. Porporato, L. Ridolfi, V. Isham, D. Coxi, Probabilistic modelling of water balance at a point: the role of climate, soil and vegetation, Proc. R. Soc. Lond. Ser. A Math. Phys. Eng. Sci. 455 (1990) (1999) 3789–3805, http://dx.doi.org/10.1098/rspa.1999.0477.

[65] F. Laio, A. Porporato, L. Ridolfi, I. Rodriguez-Iturbe, Plants in water-controlled ecosystems: active role in hydrologic processes and response to water stress: II. Probabilistic soil moisture dynamics, Adv. Water Resour. 24 (7) (2001) 707–723, http://dx.doi.org/10.1016/S0309-1708(01)00005-7.

[66] G. Botter, A. Porporato, I. Rodriguez-Iturbe, A. Rinaldo, Basin-scale soil moisture dynamics and the probabilistic characterization of carrier hydrologic flows: Slow, leaching-prone components of the hydrologic response, Water Resour. Res. 43 (2) (2007) http://dx.doi.org/10.1029/2006WR005043.

[67] S. Fatichi, V.Y. Ivanov, E. Caporali, A mechanistic ecohydrological model to investigate complex interactions in cold and warm water-controlled environments: 1. Theoretical framework and plot-scale analysis, J. Adv. Modelling Earth Syst. 4 (2) (2012) M05002, http://dx.doi.org/10.1029/2011MS000086.

[68] D.B. Stephens, Vadose Zone Hydrology, CRC Press, Boca Raton, 1995, http://dx.doi.org/10.1201/9780203734490.

[69] S.Z. Husain, S. Bélair, S. Leroyer, Influence of soil moisture on urban microclimate and surface-layer meteorology in Oklahoma City, J. Appl. Meteorol. Climatol. 53 (1) (2014) 83–98, http://dx.doi.org/10.1175/JAMC-D-13-0156.1.

[70] J.L. Santiago, A. Martilli, A dynamic urban canopy parameterization for mesoscale models based on computational fluid dynamics Reynolds-Averaged Navier-Stokes microscale simulations, Bound.-Layer Meteorol. 137 (3) (2010) 417–439, http://dx.doi.org/10.1007/s10546-010-9538-4.

[71] B. Bueno Unzeta, An Urban Weather Generator Coupling a Building Simulation Program with an Urban Canopy Model (Ph.D. thesis), Massachusetts Institute of Technology, Cambridge, 2010.

[72] B. Bueno, L.K. Norford, G. Pigeon, R. Britter, Combining a detailed building energy model with a physically-based urban canopy model, Bound.-Lay. Meteorol. 140 (3) (2011) 471–489, http://dx.doi.org/10.1007/s10546-011-9620-6.

[73] B. Bueno, G. Pigeon, L.K. Norford, K. Zibouche, C. Marchadier, Development and evaluation of a building energy model integrated in the TEB scheme, Geosci. Model Dev. 5 (3) (2012) 433–448, http://dx.doi.org/10.5194/gmd-5-433-2012.

[74] M. Moradi, The Vertical City Weather Generator (Ph.D. thesis), University of Guelph, Guelph, 2021.

[75] A.A. Aliabadi, M. Moradi, R.M. McLeod, D. Calder, R. Dernovsek, How much building renewable energy is enough? The Vertical City Weather Generator (VCWG v1.4.4), Atmosphere 12 (7) (2021) 882, http://dx.doi.org/10.3390/atmos12070882.

[76] A. Christen, R. Vogt, Energy and radiation balance of a central European city, Int. J. Climatol. 24 (11) (2004) 1395–1421, http://dx.doi.org/10.1002/joc.1074.

[77] M.W. Rotach, R. Vogt, C. Bernhofer, E. Batchvarova, A. Christen, A. Clappier, B. Feddersen, S.E. Gryning, G. Martucci, H. Mayer, V. Mitev, T.R. Oke, E. Parlow, H. Richner, M. Roth, Y.A. Roulet, D. Ruffieux, J.A. Salmond, M. Schatzmann, J.A. Voogt, BUBBLE–an Urban boundary layer meteorology project, Theor. Appl. Climatol. 81 (3) (2005) 231–261, http://dx.doi.org/10.1007/s00704-004-0117-9.

[78] B. Crawford, A. Christen, Spatial source attribution of measured urban eddy covariance CO_2 fluxes, Theor. Appl. Climatol. 119 (3) (2015) 733–755, http://dx.doi.org/10.1007/s00704-014-1124-0.

[79] G. Mussetti, D. Brunner, S. Henne, J. Allegrini, E.S. Krayenhoff, S. Schubert, C. Feigenwinter, R. Vogt, A. Wicki, J. Carmeliet, COSMO-BEP-Tree v1.0: a coupled urban climate model with explicit representation of street trees, Geosci. Model Dev. 13 (3) (2020) 1685–1710, http://dx.doi.org/10.5194/gmd-13-1685-2020.

[80] J. Yang, E. Bou-Zeid, Should cities embrace their heat islands as shields from extreme cold? J. Appl. Meteorol. Climatol. 57 (6) (2018) 1309–1320.

[81] A.A. Aliabadi, Theory and Applications of Turbulence: A Fundamental Approach for Scientists and Engineers, Amir A. Aliabadi Publications, Guelph, Ontario, Canada, 2018.

[82] T. Kawai, M.K. Ridwan, M. Kanda, Evaluation of the simple urban energy balance model using selected data from 1-yr flux observations at two cities, J. Appl. Meteorol. Climatol. 48 (4) (2009) 693–715, http://dx.doi.org/10.1175/2008JAMC1891.1.

[83] K.W. Oleson, G.B. Bonan, J. Feddema, M. Vertenstein, C.S.B. Grimmond, An urban parameterization for a global climate model. Part I: Formulation and evaluation for two cities, J. Appl. Meteorol. Climatol. 47 (4) (2008) 1038–1060, http://dx.doi.org/10.1175/2007JAMC1597.1.

[84] A.A. Aliabadi, M. Moradi, R.A.E. Byerlay, The budgets of turbulence kinetic energy and heat in the urban roughness sublayer, Environ. Fluid Mech. 21 (4) (2021) 843–884, http://dx.doi.org/10.1007/s10652-021-09800-x.

[85] M. Best, C.S.B. Grimmond, Analysis of the seasonal cycle within the first international urban land-surface model comparison, Bound.-Lay. Meteorol. 146 (3) (2013) 421–446, http://dx.doi.org/10.1007/s10546-012-9769-7.

[86] S. Kotthaus, C.S.B. Grimmond, Energy exchange in a dense urban environment-Part I: Temporal variability of long-term observations in central London, Urban Clim. 10 (2014) 261–280, http://dx.doi.org/10.1016/j.uclim.2013.10.002.

[87] A. Christen, F. Meier, D. Scherer, High-frequency fluctuations of surface temperatures in an urban environment, Theor. Appl. Climatol. 108 (1) (2012) 301–324, http://dx.doi.org/10.1007/s00704-011-0521-x.

[88] W. Morrison, S. Kotthaus, C.S.B. Grimmond, A. Inagaki, T. Yin, J.-P. Gastellu-Etchegorry, M. Kanda, C.J. Merchant, A novel method to obtain three-dimensional urban surface temperature from ground-based thermography, Remote Sens. Environ. 215 (2018) 268–283, http://dx.doi.org/10.1016/j.rse.2018.05.004.

[89] D.J. Sailor, A review of methods for estimating anthropogenic heat and moisture emissions in the urban environment, Int. J. Climatol. 31 (2) (2011) 189–199, http://dx.doi.org/10.1002/joc.2106.

[90] S.I. Bohnenstengel, I. Hamilton, M. Davies, S.E. Belcher, Impact of anthropogenic heat emissions on London's temperatures, Q. J. R. Meteorol. Soc. 140 (679) (2014) 687–698, http://dx.doi.org/10.1002/qj.2144.

[91] J. Marsalek, B.J. Cisneros, M. Karamouz, P.-A. Malmquist, J.A. Goldenfum, B. Chocat, Urban Water Cycle Processes and Interactions: Urban Water Series-UNESCO-IHP, Vol. 2, CRC Press, Paris, 2008.

[92] V.G. Mitchell, T.A. McMahon, R.G. Mein, Components of the total water balance of an urban catchment, Environ. Manag. 32 (6) (2003) http://dx.doi.org/10.1007/s00267-003-2062-2, 735–746.

[93] C.S.B. Grimmond, T.R. Oke, Urban water balance: 2. Results from a suburb of Vancouver, British Columbia, Water Resour. Res. 22 (10) (1986) 1404–1412, http://dx.doi.org/10.1029/WR022i010p01404.

[94] Y. He, H. Yu, A. Ozaki, N. Dong, Thermal and energy performance of green roof and cool roof: A comparison study in Shanghai area, J. Cleaner Prod. 267 (2020) 122205, http://dx.doi.org/10.1016/j.jclepro.2020.122205.

[95] A.M. Coutts, E. Daly, J. Beringer, N.J. Tapper, Assessing practical measures to reduce urban heat: Green and cool roofs, Build. Environ. 70 (2013) 266–276, http://dx.doi.org/10.1016/j.buildenv.2013.08.021.

[96] A. Ganguly, D. Chowdhury, S. Neogi, Performance of building roofs on energy efficiency-A review, Energy Procedia 90 (2016) 200–208, http://dx.doi.org/10.1016/j.egypro.2016.11.186.

[97] F. Salamanca, M. Georgescu, A. Mahalov, M. Moustaoui, A. Martilli, Citywide impacts of cool roof and rooftop solar photovoltaic deployment on near-surface air temperature and cooling energy demand, Bound.-Lay. Meteorol. 161 (1) (2016) 203–221, http://dx.doi.org/10.1007/s10546-016-0160-y.

[98] E.S. Krayenhoff, A.M. Broadbent, L. Zhao, M. Georgescu, A. Middel, J.A. Voogt, A. Martilli, D.J. Sailor, E. Erell, Cooling hot cities: A systematic and critical review of the numerical modelling literature, Environ. Res. Lett. (2021) http://dx.doi.org/10.1088/1748-9326/abdcf1.

[99] I.D. Stewart, T.R. Oke, Local climate zones for urban temperature studies, Bull. Am. Meteorol. Soc. 93 (12) (2012) 1879–1900, http://dx.doi.org/10.1175/BAMS-D-11-00019.1.

[100] T.R. Oke, City size and the urban heat island, Atmos. Environ. (1967) 7 (8) (1973) 769–779, http://dx.doi.org/10.1016/0004-6981(73)90140-6.

[101] S. Fatichi, The Modeling of Hydrological Cycle and its Interaction with Vegetation in the Framework of Climate Change (Ph.D. thesis), Technische Universität Braunschweig, Braunschweig, 2010.

[102] E.S. Krayenhoff, A Multi-Layer Urban Canopy Model for Neighbourhoods with Trees (Ph.D. thesis), University of British Columbia, Vancouver, 2014, http://dx.doi.org/10.14288/1.0167084.

[103] V. Mahat, D.G. Tarboton, N.P. Molotch, Testing above-and below-canopy representations of turbulent fluxes in an energy balance snowmelt model, Water Resour. Res. 49 (2) (2013) 1107–1122.

[104] A. Martilli, J.L. Santiago, CFD simulation of airflow over a regular array of cubes. Part II: analysis of spatial average properties, Bound.-Lay. Meteorol. 122 (3) (2007) 635–654, http://dx.doi.org/10.1007/s10546-006-9124-y.

[105] N. Nazarian, E.S. Krayenhoff, A. Martilli, A one-dimensional model of turbulent flow through "urban" canopies (MLUCM v2.0): updates based on large-eddy simulation, Geosci. Model Dev. 13 (3) (2020) 937–953, http://dx.doi.org/10.5194/gmd-13-937-2020.